CrossMark

ORIGINAL PAPER

Chitosan as an eco-friendly inhibitor for copper corrosion in acidic medium: protocol and characterization

A. Jmiai · B. El Ibrahimi · A. Tara · R. Oukhrib · S. El Issami ·
O. Jbara · L. Bazzi · M. Hilali

Abstract Natural biopolymer chitosan organic compound (COC) has been used as a copper corrosion inhibitor in molar hydrochloric medium. This study was conducted by weight loss, polarization curves and electrochemical impedance spectroscopy measurements. Scanning electron microscopy, energy dispersive X-ray spectrometry and atomic force microscopy studies were used to characterize the surface of uninhibited and inhibited copper specimens. The study of the temperature effect was carried out to reveal the chemical nature of adsorption. The inhibition efficiency tends to increase by increasing inhibitor concentration to reach a maximum of 87% at 10^{-1} mg L^{-1}. The values of inhibitor efficiency estimated by different electrochemical and gravimetric methods indicate the performance of copper in HCl medium containing COC. Adsorption of COC was found to follow the Langmuir adsorption isotherm. In order to get a better understanding of the relationship between the inhibition efficiency and molecular structure of COC, quantum chemical and molecular dynamics simulation approaches were performed to get a better understanding of the relationship between the inhibition efficiency and molecular structure of chitosan.

Introduction

Copper and its alloys are the most used in many industrial applications materials, more particularly in the chemical industries, power plants, in heating and cooling systems and in the electronics industry. The choice of this metal is justified by its mechanical properties, essentially its conductive properties, and its lesser cost than other more conductive metals such as gold or silver (Núñez et al. 2005; Suzuki et al. 2006; Wang et al. 2015; Zhang et al. 2016). In the literature most studies that are done consider that chloride ions are responsible for the dissolution of cuprous materials and its alloys in hydrochloric acid (Antonijević et al. 2005; Simonović et al. 2014; Zhang et al. 2016). The use of inhibitors is found to be one of the most practical methods for protection against corrosion, particularly in acidic media (Ashassi-Sorkhabi et al. 2008). Good copper corrosion-inhibiting properties exhibited by organic compounds, are known for their functional polar groups (i.e., O, N and S atoms). The

A. Jmiai · B. El Ibrahimi (✉) · R. Oukhrib ·
S. El Issami · L. Bazzi · M. Hilali
Laboratory of Materials and Environmental, Faculty of
Sciences, IBN ZOHR University, PB 8106, Dakhla,
Agadir, Morocco
e-mail: brahimmhm@gmail.com

A. Tara · O. Jbara
Laboratory of Engineering and Materials Science,
University of Reims, PB 1039, 51687 Reims, France

molecules of these polar groups can become strongly adsorbed on the metal surface to slow the copper corrosion process placed in an acid contacting medium (Lebrini et al. 2005; Sherif and Park 2006a; Tan et al. 2006; Barouni et al. 2008). The use of amino acids and derivatives of azoles as inhibitors against corrosion of copper and its alloys have given the best results (Subramanian and Lakshminarayanan 2002; Lebrini et al. 2005; Zhang et al. 2008a; Antonijević et al. 2009; Finšgar and Milošev 2010; Khaled 2010; Khan et al. 2015). Nevertheless, azoles are toxic inhibitors and are classified as environmental pollutants (Gomma 1998; Simonović et al. 2014). In our previous works we have mentioned the use of some amino acids (i.e., cysteine and lysine) and triazole derivatives for inhibition of copper in an acidic medium (Barouni et al. 2008; El Ibrahimi et al. 2016).

Natural polymer such as chitosan (i.e., N-deacetylated derivatives of chitin) may also be used as an inhibitor of copper corrosion. The main sources exploited to get this biopolymer are two marine crustaceans, shrimp and crabs. Many researchers studied the corrosion inhibition behavior of metals by chitosan biopolymers and their derivatives in acid solutions (Cheng et al. 2007; El-Haddad 2013; Alsabagh et al. 2014; Liu et al. 2015; Sangeetha et al. 2015; Menaka and Subhashini 2016; Umoren and Eduok 2016). Chitosan is known to have good complexing ability; the –NH$_2$ groups on the chain are involved in specific interactions with metals (Rhazi et al. 2002).

The aim of this study is then to investigate the abilities of chitosan organic compound (COC) to inhibit copper corrosion in a 1M HCl solution using gravimetric and electrochemical methods. The characterization of the morphology and roughness of surface of copper samples, inhibited and uninhibited, is based on scanning electron microscopy (SEM), energy dispersive X-ray spectrometry (EDX) and atomic force microscopy (AFM). To investigate the relationship between molecular structure of the inhibitor and its inhibition effect, quantum chemical calculations based on the density functional theory (DFT) are implemented.

In order to get more information about the interaction between investigated biopolymers and the substrate surface, molecular dynamics (MD) simulations were performed by using the Adsorption Locator module implemented in the Materials Studio 6.0

software (Kirkpatrick et al. 1983; Frenkel and Smit 2002).

Methodologies

Materials and chemicals preparation

For electrochemical measurements, an electrochemical cell with a three-electrode configuration was used. The working electrode, which was made of copper cylinder rod (99.99%), was sealed with Araldite epoxy glue resin so that only the circular cross-section (1 cm^2) of the rod was exposed. Before each experiment, the electrode surface was abraded with SiC abrasive papers of respectively grade 600 and 1200. A platinum foil and an Hg/Hg$_2$Cl$_2$ electrode "Saturated Calomel Electrode (SCE)" in saturated KCl, were used as counter and reference electrodes, respectively.

The copper coupons with dimensions of 2.4 cm length, 1.6 cm width, and 0.02 cm thickness with an exposed total area of 7.7 cm^2 were used for weight loss measurements (gravimetric method).

Before starting the experiment, copper samples were washed with distilled water, degreased in acetone and then dried at room temperature.

For both methods, the test solutions (1M Hydrochloric acid solution provided by Sigma Aldrich), were prepared by diluting 35–37% analytical HCl with distilled water. Chitosan (Mol. Wt. = 5000) was purchased from Sigma–Aldrich Co. Ltd. with a deacetylation content = 80%. The concentrations of inhibitor ranged from 5.10^{-3} to 5.10^{-1} (mg/L) and were prepared from a mother concentration (0.5 g/L).

Gravimetric method

Weighed copper specimens were immersed in 100 ml of a 1M HCl solution with and without addition of different concentrations of inhibitor. Several immersion times are considered at different temperatures (298, 308, 318, and 328 ± 1 K) using a temperature-controlled water bath. The specimens were weighed before and after immersion, and the weight differences were measured. For reasons of reproducibility, the measurements were repeated three times for each concentration and temperature. The average of weight losses were then taken to calculate different corrosion

parameters such as the corrosion rate (C_R) in mg cm^{-2} h^{-1} given by:

$$C_R = \frac{\Delta W}{t} \qquad (1)$$

where ΔW is the mass loss (mg cm^{-2}) and "t" is the immersion time (h).

Electrochemical methods

All electrochemical measurements were carried out using a Potentiostat/Galvanostat (Voltalab model PGZ301). The findings are plotted and analyzed by the software VoltaMaster 4. First of all, we make measurements of the open circuit potential (E_{ocp}), by the variation of electrode potential with time until the E_{ocp} stabilizes. The polarization (current–potential) curves were determined by changing the electrode potential (−500 to +250 mV with respect to SCE) with a scanning speed of 1 mV/s understatic conditions. The data were plotted and analyzed using software VoltaMaster 4. The electrochemical impedance spectroscopy (EIS) measurements were performed at corrosion potentials (E_{corr}) over a frequency range of 100 kHz–25 mHz with an wave amplitude of 10 mV, and impedance data were obtained at a rate of 20 points per decade change in frequency. These last were analyzed with the ZSIM from EC-Lab Software Version 11.00 and equipped with the appropriate equivalent circuits.

Surface morphology and elemental composition

The surface of a copper sample was immersed in 1M HCl for 24 h in the absence and presence of 10^{-1} mg/L of inhibitor and first examined by a digital camera (CANON) and then characterized by the Jeol JSM-6460LA SEM and associated EDX spectrometer. These investigations give the surface morphology and the elemental composition of the species formed on the metal surface. The AFM images of polished, uninhibited and inhibited copper samples were carried out using an AFM type Intergated Dynamics Engineering model D-65479 Raunheim nanoscope.

Density functional theory

Full geometrical optimizations of the studied molecules were conducted using density functional theory

(DFT) in gas and aqueous phase with the Becke's three parameter exchange functional with the Lee–Yang–Parr nonlocal correlation functional (B3LYP) and with the 6-31G++(2d,p) basis set as implemented in the Gaussian 09 program package (Lee et al. 1988; Frisch et al. 2009).

Some quantum chemical parameters, that influence electronic interaction enter surface atoms and inhibitor. These are the energy, E_{HOMO}, of the highest occupied molecular orbital (HOMO), the energy, E_{LUMO}, of the lowest unoccupied molecular orbital (LUMO) and the energy gap (i.e., $\Delta E = E_{HOMO} - E_{LUMO}$). According to the HOMO and LUMO energies, we can determine the electron affinity (I) and the ionization potential (A), as follows (Geerlings et al. 2003):

$$I = -E_{HOMO} \qquad (2)$$

$$A = -E_{LUMO} \qquad (3)$$

The absolute electronegativity (χ) and chemical hardness (η) that measure the resistance of an inhibitor molecule to a charge transfer (Pearson 1988) are respectively given by the following equations:

$$\chi = \frac{I + A}{2} \qquad (4)$$

$$\eta = \frac{I - A}{2} \qquad (5)$$

The softness (σ) (i.e., the inverse of the hardness) which describes the capacity of a molecule or group of molecules to receive electrons is given by (Pearson 1988):

$$\sigma = \frac{1}{\eta} \qquad (6)$$

The number of transferred electrons (ΔN), is an important theoretical parameter given by the following equation (Pearson 1988);

$$\Delta N = \frac{\chi_{Cu} - \chi_{inh}}{2(\eta_{Cu} + \eta_{inh})} \qquad (7)$$

where χ_{Cu} and χ_{inh}, are the absolute electronegativity of copper and inhibitor molecule; η_{Cu} and η_{inh} are the absolute hardness of copper and the inhibitor molecule, respectively. The theoretical values of $\chi_{Cu} = 4.48$ eV/mol and $\eta_{Cu} = 0$ eV/mol are data used for the calculation of ΔN (Pearson 1988; Wazzan 2015).

Molecular simulation dynamic

A molecular simulation study was performed employing the Materials Studio 6.0 software package to simulate the adsorption structure of the COC (the molecule is shown in Fig. 1). This simulation was carried out with a single molecule (in gas) on the Cu (111) crystal surface in a simulation box (84.35 Å × 84.35 Å × 74.61 Å) with periodic boundary conditions. The copper surface was modeled with an eight-layer slab model, each layer containing 64 copper atoms representing an (8 × 8) cell, and a great vacuum region with a thickness of 60 Å was built above the Cu (111) plane. The COMPASS (an ab initio) force field was employed to optimize the structure of all components of the system. The electrostatic potential energy was calculated by the Ewald summation technique, and the van der Waals potential energy was calculated by the atom based technique.

Results and discussion

Electrochemical methods

Open circuit potential (OCP) measurements

Another way for defining domains of corrosion is to vary the E_{OCP} over time to know the stabilization of the potential (Hassan et al. 2007). Figure 2 shows the open circuit potential–time ($E_{OCP} = f(t)$) curve for a copper electrode immersed in an aerated 1M HCl solution without and with addition of different concentrations of COC ranging from $5 \cdot 10^{-3}$ to 10^{-1} mg L^{-1}. The results show that the potential of copper without inhibitor (Blank) stabilizes at -250 mV value. The OCP for the copper in acid

medium is heading for a more negative potential indicating a corrosion process related with the work of chloride ions (Ismail 2007). Furthermore, the initial potential was shifted towards more negative values as COC concentration increases. This can be attributed to the adsorption of chitosan molecules onto active corrosion sites on the metal surface. The same behavior was observed by Mahmoud El-Haddad (2013) that found that the corrosion potential shifts to the cathode potential.

Polarization curve and electrochemical impedance measurements

The electrochemical methods allow us to determine the corrosion phenomena. Figure 3 shows stationary (a) and transient (b) curves of copper in aerated hydrochloric medium. The anode part of the polarization curve (a) shows three prominent regions: First, a region growing at current density from a potential at -256.71 to -42.64 mV passing through a peak current density (J_{peak}), this is because the dissolution by oxidation of Cu metal into Cu(I) (Eq. 8) (Larabi et al. 2006; Sherif and Park 2006b, c). Afterwards, a region of currents dropping to a minimum ($J_{min} = -2.37$ A cm^{-2}) is observed. This last fall of the current density could be due to the formation of CuCl (Tromans and Silva 1996; Sherif and Park 2006c) as explained by the reaction (Eq. 9). Finally, a region of abrupt increase in current density that leads to a limit value (Jlim) can be attributed to formation of CuCl$_2^-$ resulting from the dissolution of copper in acid followed by its oxidation to Cu(II) (see Eq. 10) (Tromans and Silva 1996; Sherif and Park 2006c). The same result was found by Larabi et al. (2006), Tromans and Silva (1996) and Zhang et al. (2008a, b).
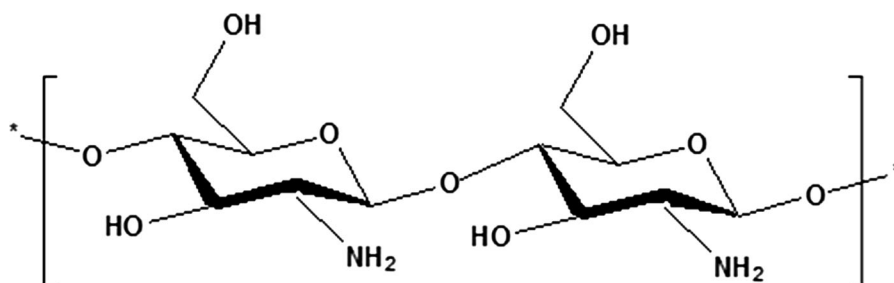
$$Cu \rightarrow Cu^+ + e^- \qquad (8)$$
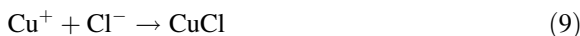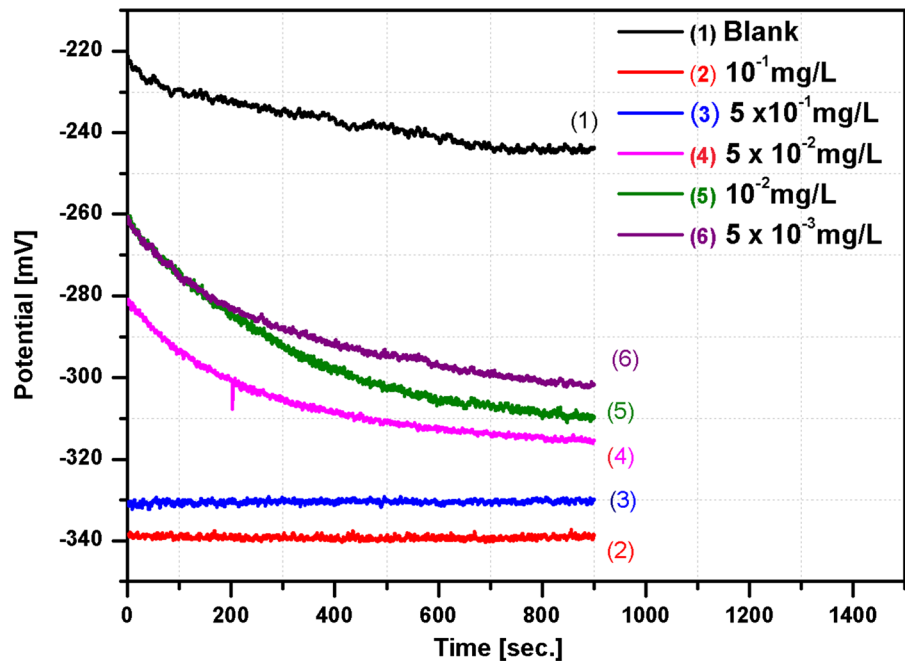
Fig. 1 Molecular structure of chitosan

Fig. 2 Open circuit potential of Cu in 1M HCl with and without inhibitor at 25 °C

$$Cu^+ + Cl^- \rightarrow CuCl \tag{9}$$

$$CuCl + Cl^- \rightarrow CuCl_2^- \tag{10}$$

The cathodic polarization curve displayed also a current plateau from −260 to −600 mV. This can be assigned to reduction of dissolved oxygen inside the aerated corrosive solution, because we work in an aerated middle (Zhang et al. 2008a, b). According to Sherif and Park (2006c), Larabi et al. (2006) and Da-Quan Zhang et al. (2008b), the chemical reaction involved in the cathode compartment is as follows: (Eq. 11)

$$4H^+ + O_2 + 4e^- \rightarrow 2H_2O \tag{11}$$
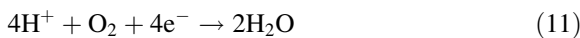
Part (b) of Fig. 3 shows the Nyquist impedance diagram of copper in 1M HCl to be uninhibited. A semicircle loop capacitive observed is generally attributed to charge transfer resistance (Sherif and Park 2006b). In the high frequency region the behavior of the corrosion of copper in uninhibited solutions may be due to rapid charge transfer of the metal dissolution in the corrosive medium (Larabi et al. 2006; Zhang et al. 2008b) as follows:

$$Cu + Cl^- \rightarrow CuCl_{ads} + 1e^- \tag{12}$$
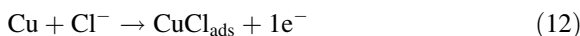
The potentiodynamic polarization curves for the copper in aerated solution of 1M HCl in the absence

and presence of different concentrations of COC at 25 °C are shown in Fig. 4. Values of the electrochemical corrosion parameters, such as corrosion potential (E_{corr}), cathodic Tafel slop (βc), anodic Tafel slop (βa), and corrosion current density (I_{corr}) are presented in Table 1. The I_{corr} and E_{corr} parameters were determined from the Tafel plots using EC-Lab software. As well, the corrosion rate (milli inches per year, mpy) was obtained as follows:

$$C_R(mpy) = \frac{I_{corr}kE_W}{dA} \tag{13}$$

where k is a constant of corrosion rate ($k = 128{,}800$ milli inches (amp cm year)), A is the area of electrode (cm^2), d is the density (g cm^{-3} = 8.92) and E_W is the equivalent weight in grams/equivalent of copper (= 31.75) (Sherif and Park 2006a). The corrosion inhibition efficiency (IE$_p$) was calculated from I_{corr} using the following equation:

$$IE_p(\%) = \frac{I_{corr} - I_{corr(inh)}}{I_{corr}} \times 100 \tag{14}$$

where I_{corr} and $I_{corr(inh)}$ indicate the corrosion current densities without and with different concentrations of the inhibitor, respectively.

From Fig. 4 and Table 2 it is seen that the addition of the inhibitor (COC) in low concentrations has an important effect on the inhibition of corrosion of
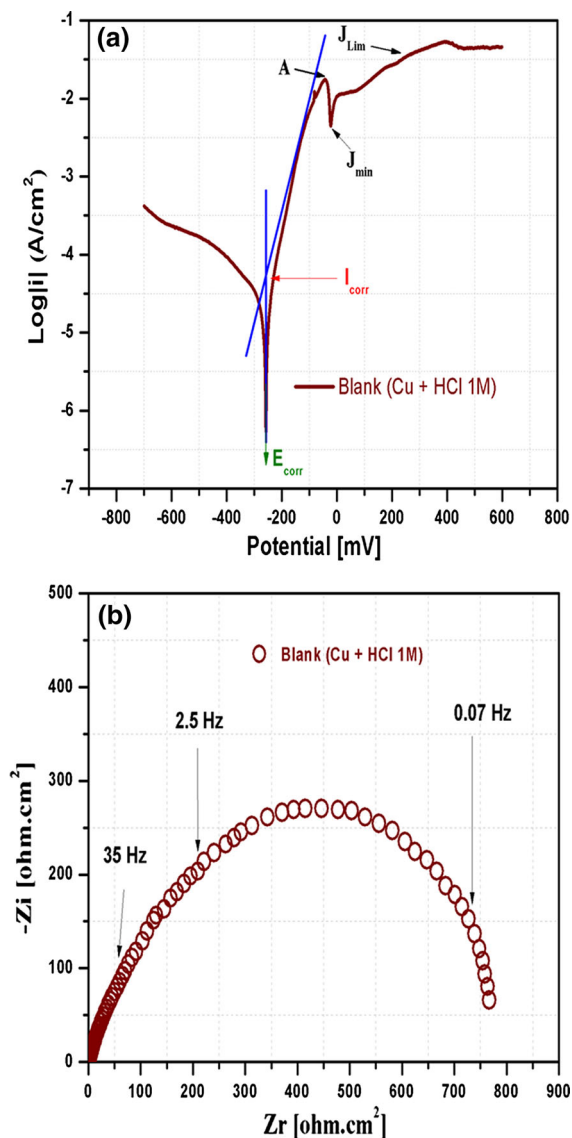
Fig. 3 Polarisation (**a**) and Nyquist (**b**) curves of copper in hydrochloric medium aerated without inhibitor (*blank*) at 25 °C

medium has a remarkable influence by the reduction of the cathodic current on the one hand and the corrosion current density (I_{corr}) on the other hand. The values of the anodic Tafel lines βa, show minor changes with the addition of COC, the C_R(mpy) decreases with increasing concentration of the inhibitor and $IE_p(\%)$ increases with concentration of the inhibitor, reaching its maximum value, 87.34%, at 10^{-1} mg/L. Because of this, is a very significant reduction in the corrosion current I_{corr}, primarily to lower attack of the chloride ion on the copper surface; this is probably due to the effect of adsorption of COC molecules on active centers of metal surface and protecting the copper surface (El-Haddad 2013, 2014; Deyab et al. 2015; Sangeetha et al. 2015; Yadav et al. 2015a; Sherif et al. 2007).

Figures 5 and 6, show, respectively, the Nyquist and Bode plots obtained for copper immersion in 1M HCl aerated solution in the absence and the presence of COC. The electrochemical equivalent circuits employed to analyze impedance spectra for Nyquist plots by EC-Lab software are shown in Fig. 7. The parameters obtained by the assembly of the equivalent circuit and the calculated inhibition efficiency are listed in Table 2. Here, Rs represents the solution resistance, R_{ct} is the charge-transfer resistance, and CPE is the constant phase element.

The single depressed capacitive half-circle represented by the impedance spectra of Fig. 5 in general is associated with charge transfer (Deyab et al. 2015). The reasoning of these imperfect semicircles is known by the "dispersing effect" that can be explained by the roughness of the metal surface (Khaled and Hackerman 2004; Liao et al. 2011; El-Haddad 2013; Deyab et al. 2015). The diameter of the capacitive loop increased in parallel with the increase in COC concentration at a value of 10^{-1} mg/L. From the Table data, the Rct values in a medium containing COC are higher than in the corrosive middle. This may be attributed to the higher surface coverage of COC on the electrode surface (Menaka and Subhashini 2016). A Nyquist plot does not show any frequency value. To overcome this shortcoming, Bode plots were developed to indicate exactly the frequency behavior of the corrosion phenomenon. The experimental Bode diagrams are displayed in two plots: magnitude and a phase plot in Fig. 6. From the plots of the amplitudes, we observe that log |Z| Increases with increasing COC concentration reaching an amplitude value of "3.8

copper in hydrochloric medium. The shift of E_{corr} towards the negative with increasing concentration of the inhibitor could be due to the decrease in the rate of the cathodic reaction (Sangeetha et al. 2015). In other words, chitosan affects the reduction of dissolved oxygen in solution (Khaled and Hackerman 2004). From Table 2, it can be seen that the modification of i-E towards cathodic branches is well done and the anodic Tafel slope is almost unchanged, which may suggest that COC is a cathodic inhibitor type. It is also noted that the addition of COC to the corrosive

Fig. 4 Potentiodynamic polarization curves for copper in aerated medium 1M HCl in the absence and presence of various concentrations of COC at 25 °C
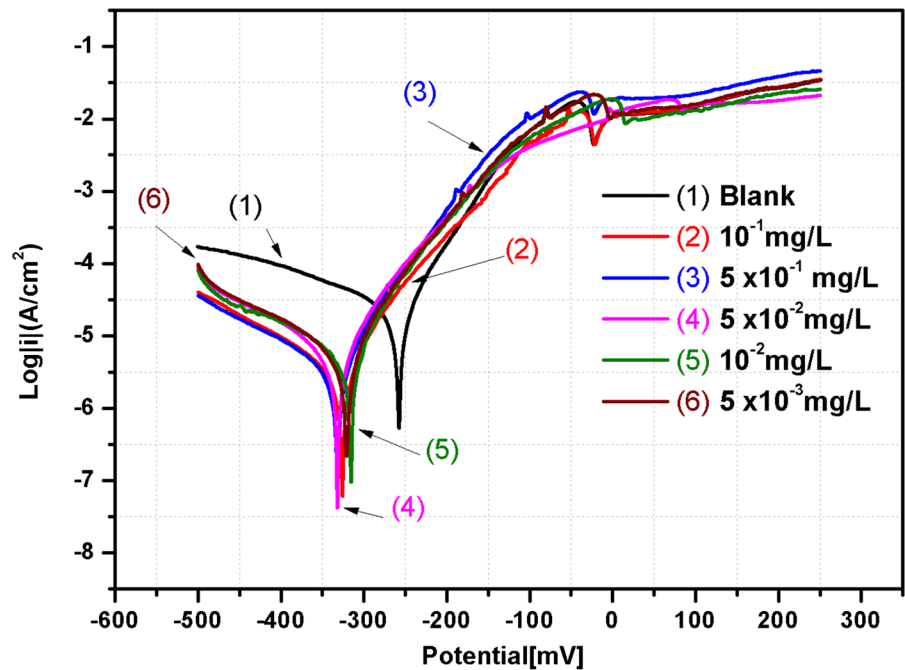

Table 1 Electrochemical parameters of copper in 1M HCl with and without COC at various concentrations and the corresponding inhibition efficiency

C (mg/L)	β_a (mv/dec)	$-\beta_c$ (mv/dec)	E_{corr}/(SCE) (mV)	I_{corr} (μA/cm^2)	CR(mpy)	IE$_p$(%)
0.0	60.90	250.10	−256.64	26.22	12.02	00.00
5×10^{-3}	73.55	232.44	−321.37	8.72	4.00	66.74
1×10^{-2}	71.86	288.77	−316.51	8.48	3.89	67.66
5×10^{-2}	72.63	179.00	−333.96	6.60	3.02	74.83
1×10^{-1}	65.26	160.88	−327.22	3.32	1.52	87.34
5×10^{-1}	63.26	205.80	−333.52	3.80	1.74	85.50

Table 2 Parameters obtained by fitting the Nyquist and Bode plots shown in (Figs. 5 and 6) with the equivalent circuit shown in Fig. 7 for a copper electrode in aerated 1M HCl solution in the absence and presence of COC at 25 °C

C (mg/L)	R_s (Ω cm^2)	R_{ct} (Ω cm^2)	CPE$_{dl}$ (μF cm^{-2})	n	IE$_I$ (%)
0.0	3.297	788.4	462	0.666	0.0
5×10^{-3}	5.557	2023.4	406	0.690	61.04
1×10^{-2}	3.860	2248.7	382	0.704	65.00
5×10^{-2}	7.063	2767	244	0.718	71.51
1×10^{-1}	3.694	5949.1	23	0.803	86.75
5×10^{-1}	8.557	4678.8	72	0.782	83.15

Ohm cm^2'' and a value of "2.8 Ohm cm^2'' for the Blank; the same thing for phase angle is greater by increasing the concentration of COC compared to uninhibited copper. This margin of magnitude and phase angles can be explained by the resistivity of this

region (horizontal line for magnitude plots a phase angle $\theta \sim 0$) in the presence of the inhibitor (Sherif et al. 2008; Fekry and Mohamed 2010).

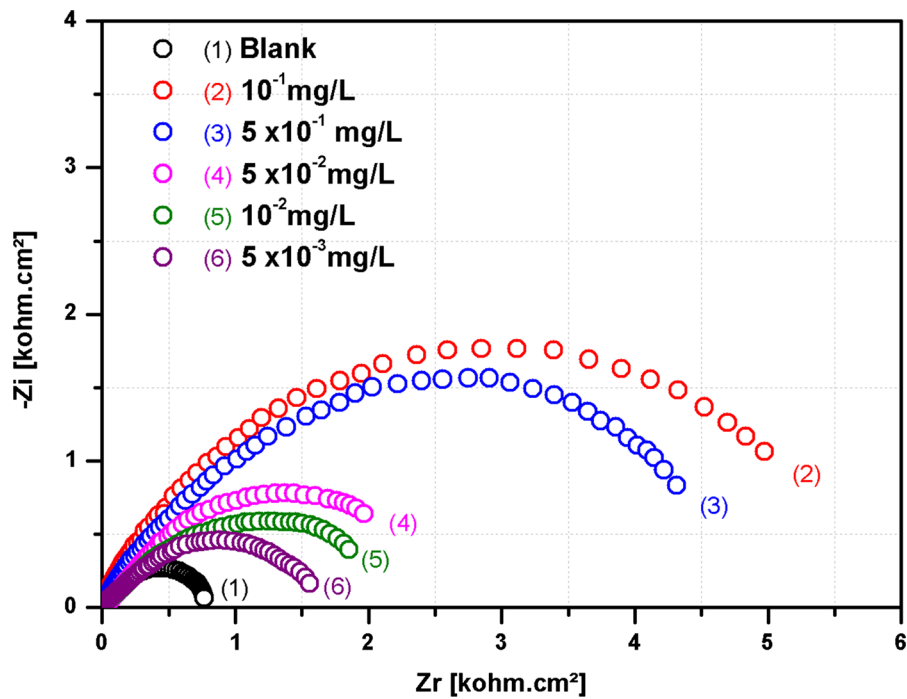The large decrease of the constant phase element (CPE$_{dl}$ = 23 μF cm^{-2}) at higher COC concentrations

Fig. 5 Nyquist plots for copper immersion in 1M HCl aerated solution with and without different concentrations of COC at 25 °C
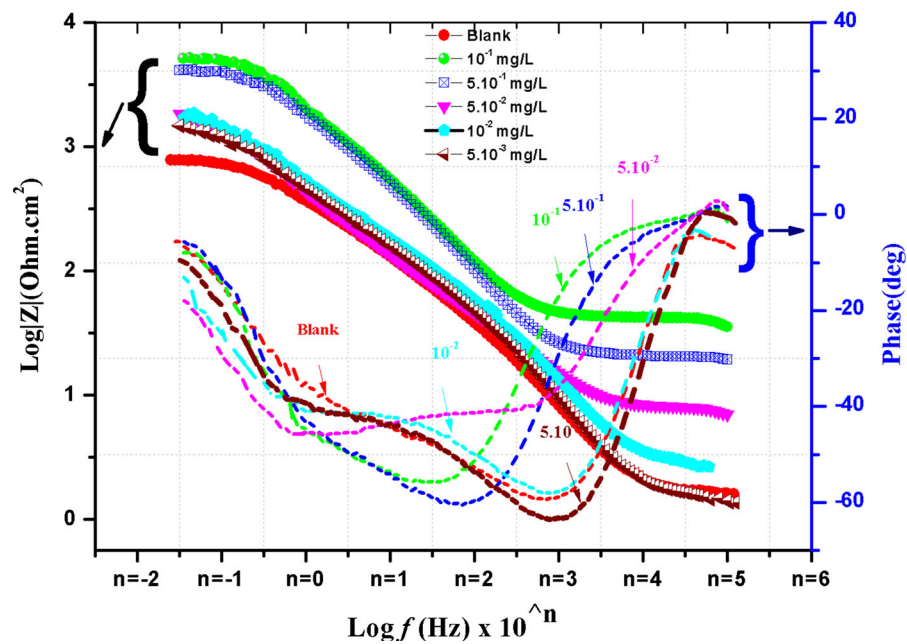

Fig. 6 Bode plots obtained for copper immersion in 1M HCl aerated solution in the absence and presence of various concentrations of COC at 25 °C
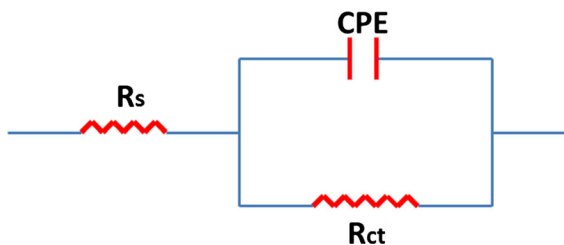
Fig. 7 Electrical equivalent circuit (Rs, solution resistance; Rct, charge transfer resistance; and CPE, constant phase element) used in fitting the experimental impedance data

is due to the limited access of the charged particles to the surface (Sherif and Park 2006b). This may be explained by the formation of a barrier which prevents the attack of chloride ions on the metal surface (Zhang et al. 2005; Deyab et al. 2015; Sangeetha et al. 2015; Yadav et al. 2015a). From Table 2 we see that the value of n changes from 0.690 to 0.803 with respect to the Blank. This is probably due to the low inhomogeneity of the metal surface bound to the adsorption of COC which blocks the active centers (Larabi et al. 2006).

The inhibition efficiency (IE_{Im} %) of copper corrosion can be calculated according to the following formula (14):

$$IE_{Im}\% = \left[1 - \left(\frac{R_{ct}}{R_{ct(Inh)}}\right)\right] \times 100 \qquad (15)$$

where $R_{ct(Inh)}$ and R_{ct} are the charge-transfer resistances with and without the inhibitor. Table 2 clearly shows that the inhibition efficiency increases with an increase of COC concentration, reaching a maximum value (86.75%) at a 10^{-1} mg L^{-1} concentration. This is in agreement with the polarization data in the same conditions.

Gravimetric method

The gravimetric method is a non-electrochemical technique involving immersion of copper specimens in electrolyte solution for a period of time. Though this method is time-consuming, it is more reliable than electrochemical techniques. Results of mass loss ΔW and corrosion rate C_R as a function of immersion time are shown in Fig. 8a, b.

We observed for pure Cu that it easily dissolved in aerated HCl 1M with immersion time, and a remarkable decrease of C_R from 0 to 30 h was followed by a

stabilization from 30 to 168 h. On the other hand, ΔW increased as a function of the immersion time for copper samples with and without inhibitor. To explain this phenomenon, in chloride medium, the copper oxidizes to Cu (I) by dissolving the metal and reacts with the free chloride ions in the acid, which leads to the formation of the CuCl compound, then transforms into a $CuCl_2^-$ complex, Sherif and Park (2006b; c) found the same results. The addition of COC to the corrosive solution slows down the attack of Cl^- ions and prevents the formation of the CuCl compound (see below SEM and EDS) (Sherif and Park 2006b; El-Haddad 2013; Liu et al. 2015; Sangeetha et al. 2015).

The inhibition or acceleration IE_W (%) was computed from the equation:

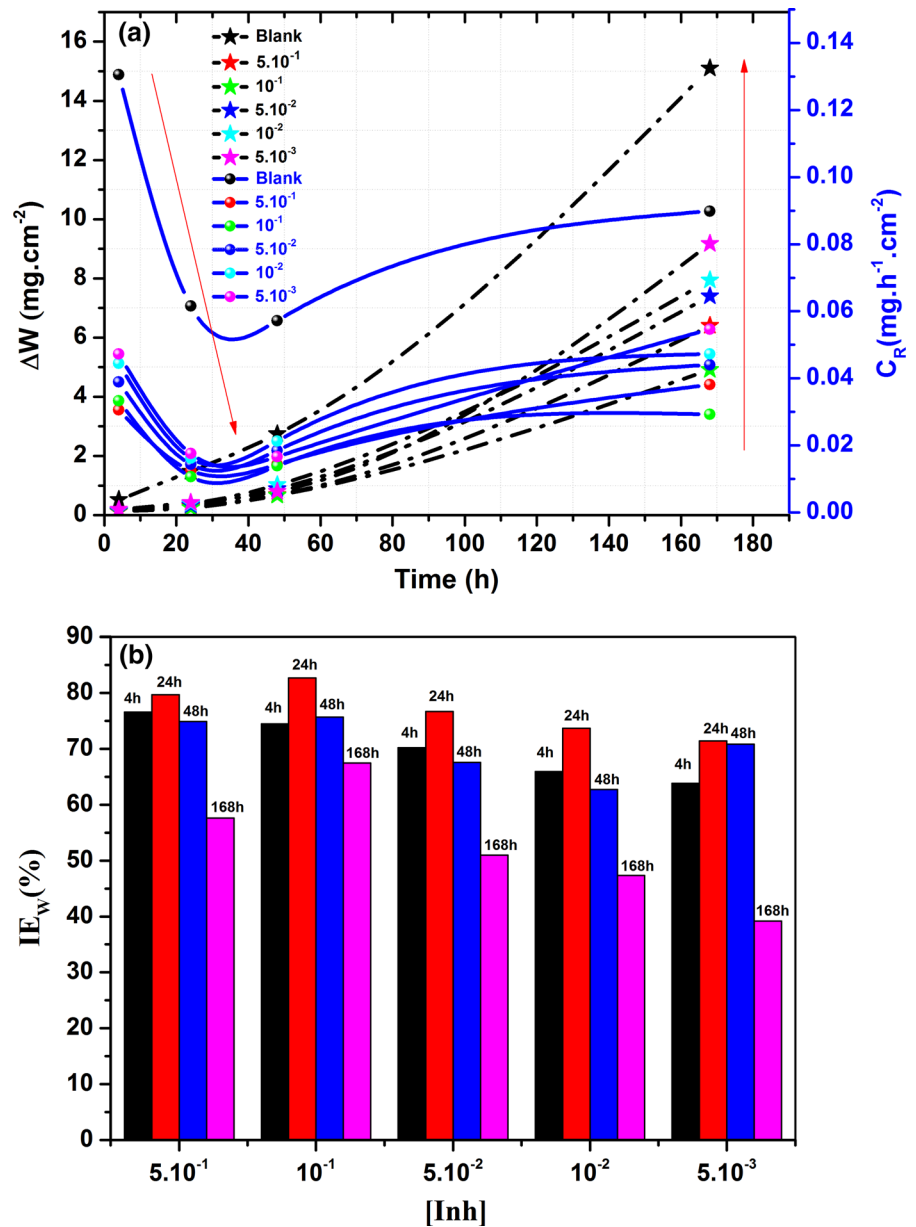$$IE_W(\%) = \frac{C_R - C_{R(inh)}}{C_R} \times 100 \qquad (16)$$

where $C_{R(inh)}$ and C_R are the corrosion rates of copper in the presence and the absence of definite concentration of inhibitor, respectively. It is revealed that the inhibition efficiency increased with the increase of inhibitor concentration and reached a maximum of 83% after 24 h of immersion in 1M HCl at 25 °C at the optimum concentration of 10^{-1} mg/L. This maximum value could be attributed to the increasing stabilization of COC on the copper surface (Arukalam et al. 2015; Tawfik 2015). These results confirm that COC inhibitor exhibited good corrosion inhibition even at low concentrations. It is worth noting that, these corrosion weight loss tests were in good agreement with impedance measurements and the polarization curves method.

Effect of temperature

Temperature is an important parameter, because it makes it possible to considering the nature of the adsorption of inhibitor on the metal surface, and to know the effect of temperature on the stability of the inhibitor.

Figure 9 presents the impedance diagram in the absence (a) and presence (b) of 10^{-1} mg/L of COC inhibitor at various temperatures. Table 3 combines the electrochemical parameters obtained. According to this Fig. 1 and Table 2, it is seen that the half-circle diameter of the capacitive loop decreases with increasing temperature for the copper electrodes in inhibited and uninhibited media (Bousskri et al. 2015).

It is clear that the RCT values in both media in the presence and absence of the COC decrease with increasing temperature and in parallel with the inhibitory efficiency decreasing. The decrease of the EI with the increase in temperature is also due to desorption of the inhibitor molecules, which reduces the capacity of the inhibitor to adsorb on the metal surface at an elevated temperature (Deyab et al. 2015; Menaka and Subhashini 2016; Sangeetha et al. 2016a).

Figure 10 shows the mass loss and the inhibition efficiency of copper with the addition of 10^{-1} mg/L of COC according to different temperatures. It is clear that the IE_w(%) decreases with increasing temperature and the weight loss increase with this condition. The increase in temperature has an influence on the chemical reactivity which confirms desorption of the inhibitor from the copper surface. This can be explained by the roughness of the metal surface due to the high temperature which slows down the
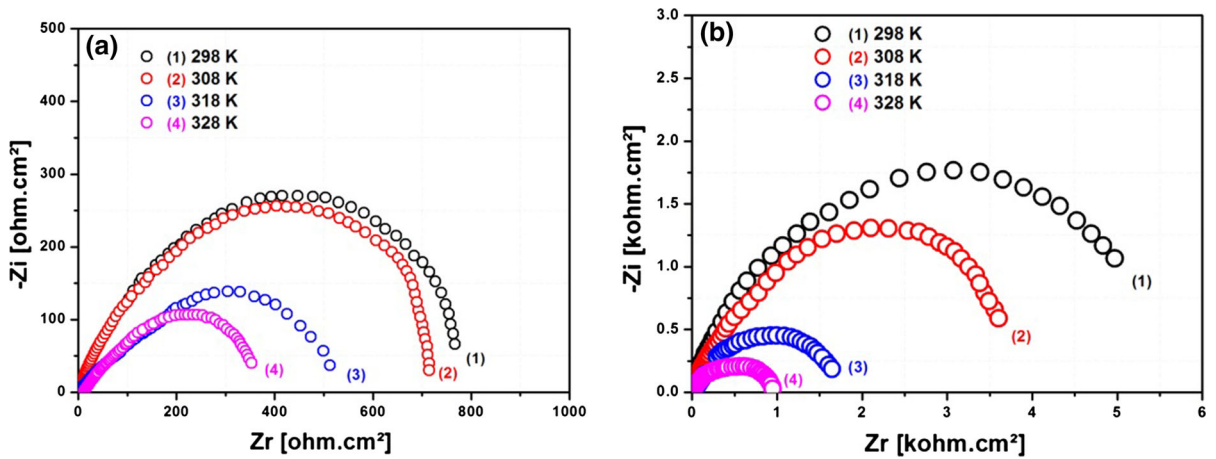
Fig. 9 **a** Nyquist diagrams for copper in 1M HCl and **b** 1M HCl + 10^{-1} mg/L of COC at different temperatures

Table 3 Thermodynamic parameters for the adsorption of COC in 1.0M HCl on copper at different temperatures

	$T°$ (K)	R_{ct} (Ω cm^2)	CPE_{dl} (μF cm^{-2})	IE_I (%)
Blank	298	788.4	462	0.0
	308	710.4	704	0.0
	318	514.8	1794	0.0
	328	388.6	3655	0.0
COC (10^{-1} mg/L)	298	5949.1	23	86.7
	308	3707	71	80.8
	318	1610	90	68.0
	328	919	480	57.7

Fig. 10 Variations of weight loss measurements and corresponding inhibition efficiency as a function of temperature of copper in 1M HCl at a concentration of 10^{-1} mg/L of COC
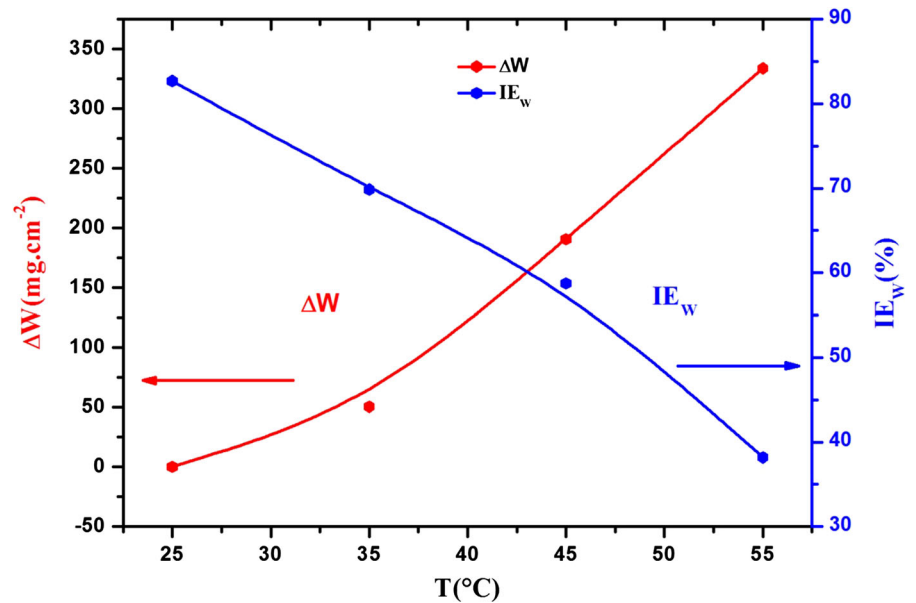
inhibitor's ability to adsorb onto the copper surface (Yadav et al. 2015a; Menaka and Subhashini 2016).

In general, according to the results obtained from the temperature effect for the both electrochemical and gravimetric methods, it was found that the inhibitory efficiency decreases with increasing temperature.

Adsorption isotherm and thermochemical parameters

To fully understand the adsorption behavior of an inhibitor towards the metallic surface, it is important to investigate adsorption modes. According to the results of the gravimetric methods, there is a direct relationship between the inhibition efficiency (IE$_W$%) and surface coverage (θ) for different concentrations of inhibitor at 25 °C.

In order to clarify the nature of the adsorption, the surface coverage values (θ) were tested graphically to allow fitting of an appropriate adsorption isotherm. As a result, the graph of C/θ with respect to C (Fig. 11) yielded a straight line with a slope nearly unitary. Langmuir, Temkin and Freundlich adsorption isotherms equations have been attempted to find their best fit to the experimental data (Bousskri et al. 2015; Sangeetha et al. 2015). Table 4 lists these equations and their linear correlation coefficients. The Langmuir adsorption isotherm was found to provide the best description of the adsorption behavior of the investigated inhibitor on the copper surface. Recall that the equation corresponding to the Langmuir adsorption isotherm is the following:
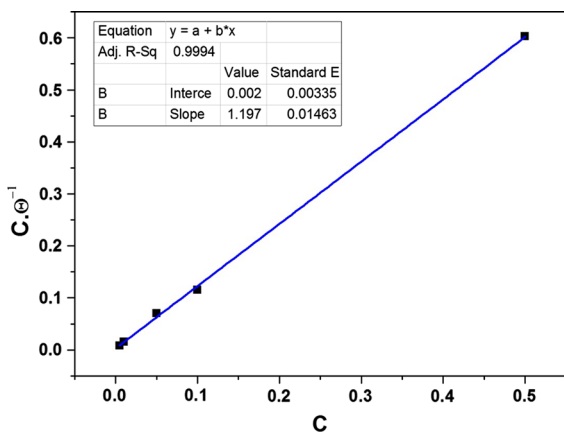

Fig. 11 Langmuir isotherm for adsorption of COC on the copper surface in 1M HCl

$$\frac{C}{\theta} = \frac{1}{K} + c \tag{17}$$

where K is the adsorption/desorption equilibrium constant and C is the corrosion inhibitor concentration in the solution.

The thermodynamic standard Gibbs free energy of adsorption ΔG_{ads}, which can characterize the interaction of adsorption molecules with a metal surface, was calculated from the equilibrium constant using the following equation (Sangeetha et al. 2015):

$$\Delta G_{ads} = -RT \ln (55.5K) \tag{18}$$

where R is the gas constant and T is the absolute temperature (K). The value of 55.5 is the concentration of water in solution in mol/L. The ΔG_{ads} value calculated from mass-loss data at 25 °C is -41.9 kJ mol^{-1}. This large negative value of ΔG_{ads} is usually characteristic of the spontaneity and stability of the layer formed by the adsorption of COC molecules on the surface of copper (El-Haddad 2013, 2014; Bousskri et al. 2015). According to the literature (Menaka and Subhashini 2016; Sangeetha et al. 2016b), if the value of ΔG_{ads} is about -20 kJ mol^{-1} then; therefore, there is an electrostatic interaction between the inhibitor and the metal surface (physical adsorption). If the value of ΔG_{ads} greater or around -40 kJ mol-1; therefore, there is a chemisorption between the inhibitor and the surface of the material. In our case ($\Delta G_{ads} = -41.9$ kJ/mol) indicates that the adsorption mechanism between the COC molecules and the copper surface is stronger and of the chemisorption type. This can be attributed to the long COC chain with active groups responsible for the great spontaneity of adsorption (Cheng et al. 2007; El-Haddad 2013; Menaka and Subhashini 2016).

Analysis of the plotting of the corrosion rate as a function of temperature makes it possible to determine other parameters such as the activation energy enthalpy and the standard entropy of the reaction to explain the corrosion process as well as the possible mechanism of inhibitor adsorption. Figure 12a presents the Arrhenius plots of the natural logarithm of the corrosion rate (Log (C_R) (mg cm^{-2} h) versus 1000/T (K^{-1}) for 1M solution of hydrochloric acid without and with addition of 10^{-1}mg/L COC. Straight lines are obtained with correlation coefficients of 0.99. The values of the slopes of these straight lines permit

Table 4 Linear correlation coefficient of different adsorption isotherm equations

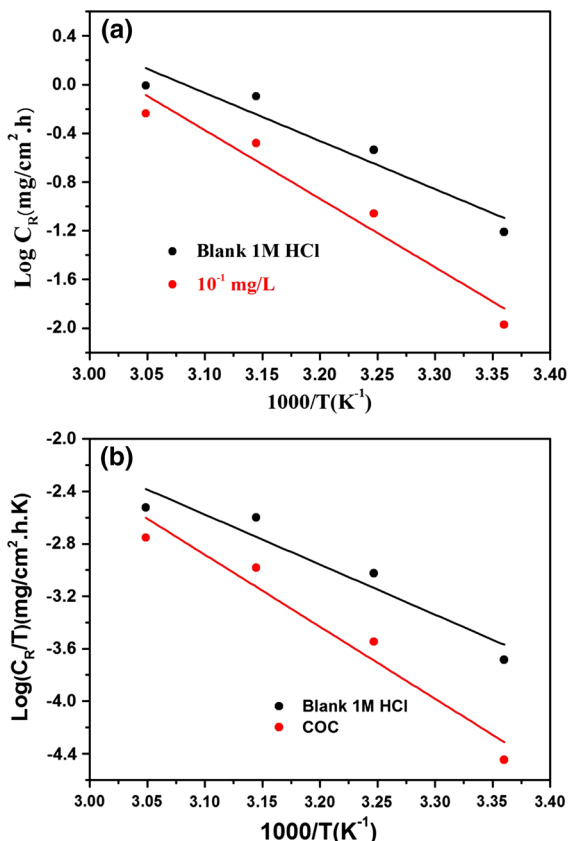| Adsorption Isotherm	Equation	Linear correlation coefficient (R^2)
Freundlich	$Ln\theta = LnK + nLnC$	0.817
Temkin	$\theta = -\frac{1}{2a}LnK - \frac{1}{2a}LnC$	0.800
Langmuir	$\frac{C}{\theta} = \frac{1}{K} + C$	0.999

Fig. 12 **a** Arrhenius plot for copper corrosion in 1M HCl in the absence and presence of 10^{-1} mg/L concentration of chitosan, **b** Transition state plot of log (C_R/T) versus 1000/T for copper corrosion in 1M HCl in the absence and presence of 10^{-1} mg/L of COC

the calculation of the Arrhenius activation energy E_a, according to:

$$Log(C_R) = -\frac{Ea}{2.303RT} + A \quad (19)$$

where R is the molar gas constant, T is the absolute temperature and A is the Arrhenius constant.

The calculated value of activation energy for the blank 1M HCl as found to be 22.54 kJ mol^{-1} is in

good agreement with literature results (17–25 kJ mol^{-1}) (Herreros et al. 1999; Habbache et al. 2009; Kim et al. 2011).

Compared to the blank solution, the value of E_a in the presence of inhibitor is 32.13 kJ/mol is greater. This higher energy value in the presence of COC indicates that the corrosion process has been changed, this may be due to the influence of the COC molecules on the adsorption mechanism, which explains the high inhibition efficiency (Fekry and Mohamed 2010; Yadav et al. 2015a; Menaka and Subhashini 2016).

The values of standard enthalpy of activation ($\Delta H°$) and standard entropy of activation ($\Delta S°$) were calculated by applying the transition state equation (Fekry and Mohamed 2010):

$$Log\left(\frac{C_R}{T}\right) = \left[\left(Log\left(\frac{R}{Nh}\right) + \left(\frac{\Delta S°}{2.303R}\right)\right)\right] - \frac{\Delta H°}{2.303RT} \quad (20)$$

where h is the Planck's constant, N is Avogadro's number, and T is the absolute temperature. In Fig. 12b a plot of Log (C_R/T) against (1000/T) is shown. The slope of the obtained straight line gives the enthalpy of adsorption $\Delta H°$.

Positive values, 105.32 and 73.15 kJ/mol of $\Delta H°$ are, respectively, obtained in the absence and presence of the inhibitor. This expresses the endothermic reaction of the copper dissolution process (Bousskri et al. 2015; Sangeetha et al. 2016b).

Surface characterization

Visual observation

To have an overall view of the state of the corroded surface, photographs of copper coupons in different configurations were taken by using a digital camera. Figure 13 shows these photographs for polished and untreated copper (without the attacking corrosive
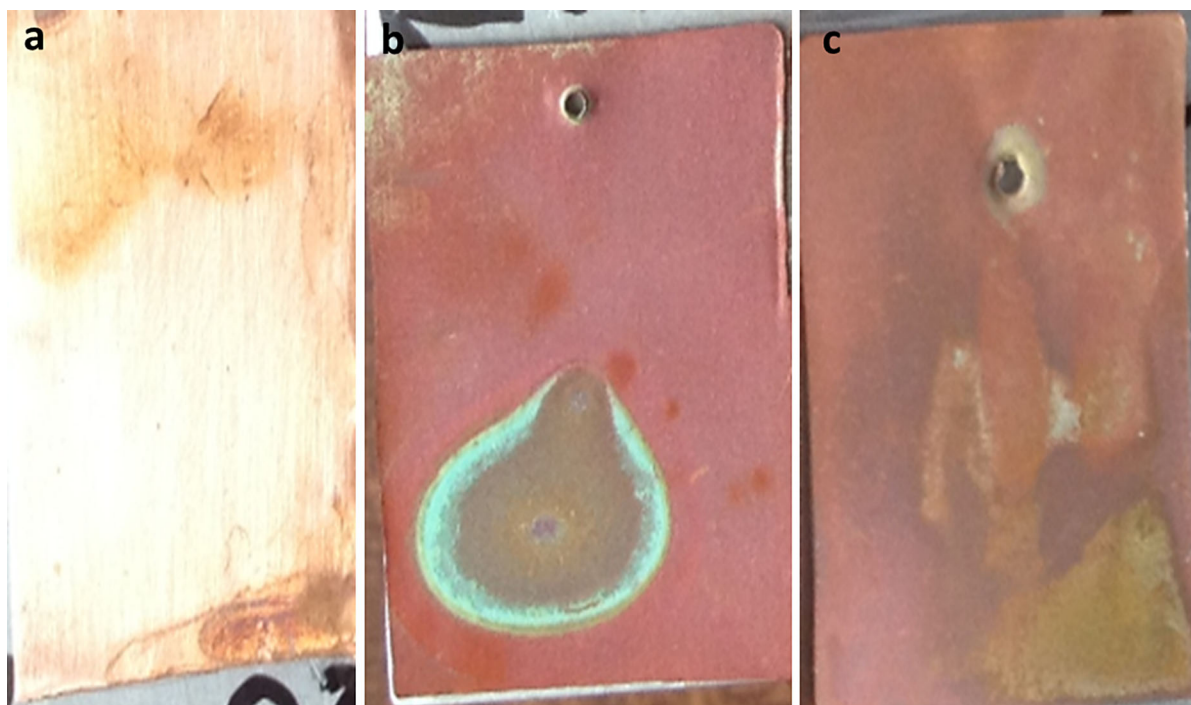
Fig. 13 Photographs of the copper coupons tested in 1M HCl solution after 24 h immersion **a** reference, **b** without and **c** with 10^{-1} mg/L COC inhibitor at 25 °C

solution) as a reference (a), after 24 h of full contact with HCl 1M without inhibitor (b) and with inhibitor (c). By analyzing the photographs we see clearly that picture (a) shows a clean copper surface while picture (b) shows a dark red color indicating a corroded surface and a green spot in the middle. The green spot corresponds to the formation of copper oxides or complex formation CuCl and/or $CuCl_2^-$ on the copper surface. The picture (c) clearly shows the non-corroded surface presenting brown and black films that can be attributed to the adsorption of the COC inhibitor (Khan et al. 2015).

SEM observation and EDS analysis

Further morphological studies of the copper surface were obtained using SEM. The results are shown in Fig. 14a–c. The morphology of the polished copper specimen before immersion in acidic solution (Fig. 14a) is very smooth and uniform, straight stripes are formed during mechanical polishing. After immersion in the corrosive solution 1M HCl without inhibitor (Fig. 14b), the surface is rough (El-Haddad 2013; Umoren and Eduok 2016) with crystalline

aggregates of a triangular shape. This shows that the surface is strongly corroded by the acidic medium resulting in corrosion products due to metal dissolution (Vathsala et al. 2010; El-Haddad 2013; Sangeetha et al. 2015; Umoren and Eduok 2016). The SEM image corresponding to the presence of COC (Fig. 14c), shows an unbroken and improved surface with the absence of triangular crystalline aggregates. The copper dissolution in this case is greatly mitigated by the adsorption of COC that prevents the formation of corrosion products (El-Haddad 2013; Sangeetha et al. 2015; Umoren and Eduok 2016). In order to get information about the composition of the surface of the copper sample in the absence and presence of inhibitors in 1M HCl solution, the EDS technique is implemented. The obtained spectra are shown in Fig. 14 (a′, b′, c′). The mass percentage contents of various elements composing studied samples, deduced from quantitative analysis of these spectra, are shown in Table 5. The analysis clearly shows that the main element constituting the polished copper sample is copper (99.03%), and residual elements, due to the surface contamination, such as O (0.73%) and C (0.04%) are also observed.
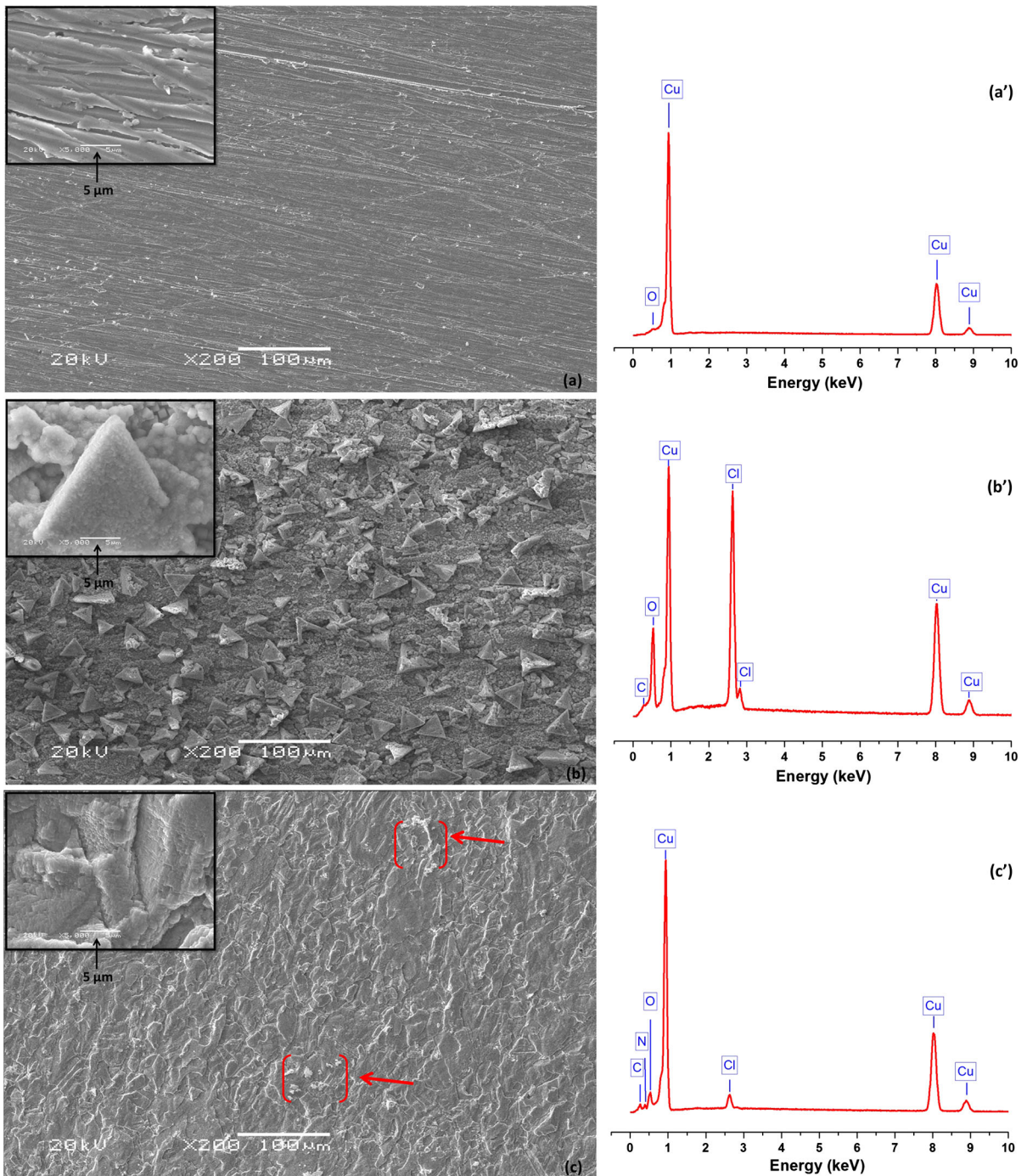
Fig. 14 SEM images (*left*) and corresponding EDS spectra (*right*) of untreated polished copper (**a**, **a′**) and after 24 h immersion without inhibitor in 1M HCl solution at 25 °C (**b**, **b′**) and with the presence of (10^{-1} mg/L) inhibitor COC (**c**, **c′**)

The mass compositions of the detected elements on the copper surface in aerated 1M HC without inhibitor are 68.22% Cu, 17.69% Cl, and 11.62% oxygen. The latter confirms the possible corrosion compound formed on the metal surface which contains the chloride that may consist of CuCl or $CuCl_2^-$ (Sherif

Table 5 Mass percentage contents of elements deduced from EDS spectra

Sample	Cu	Cl	O	C	N
Pure Cu (reference)	99.03	–	0.14	0.63	–
Cu + 1M HCl (blank)	68.22	17.69	11.62	2.47	–
10^{-1} mg/L(COC) + Cu + 1M HCl	94.12	1.89	1.94	1.03	1.02

and Park 2006a, b; Deyab et al. 2015). This result is in agreement with electrochemical and gravimetric previous studies, indicating a significant increase of the copper dissolution.

For the copper immersed in acidic solution with the presence of inhibitor COC, not only the percentage of copper (94.12%) is higher than that of the copper attacked without inhibitor, a characteristic additional signal of the nitrogen N (1.02%) is observed. This indicates that the COC molecules were directly adsorbed onto the copper surface to create a protective barrier against chloride ions (El-Haddad 2013; Deyab et al. 2015; Liu et al. 2015) which greatly reduces the possibility of forming copper chloride complexes and limits corrosion of copper Cu. In comparing this case to the absence of inhibitor chloride ions, they are responsible for the metal dissolution with very low Cl (1.89%) and oxygen O (1.94%). This assures the slowing down of the corrosion product and oxide formed on the surface of the copper (Sherif and Park 2006b; Menaka and Subhashini 2016). Note that the EDS analysis is in good agreement with the results of polarization and impedance measurements we have taken before.

AFM observation

Another choice for studying the effect of inhibitors on the corrosion rate at the electrode/electrolyte interface (Satapathy et al. 2009) is to investigate the surface morphology at nano- to micro-scale using AFM technique. The surface roughness of the copper specimens before and after immersion in 1M HCl solution without and with (10^{-1} mg/L) COC at 25 °C was examined and the corresponding images are shown in Fig. 15.

AFM images of polished copper sample (a, a′) reveal that the sample before immersion has a regular surface with certain imperfections such as small holes and polishing scratches as a result of the abrading

treatment. The height of the sample surface is $z = 361.1$ nm indicate that the surface of metal roughness (Rocca et al. 2001; Wang et al. 2011; Mourya et al. 2014; Yadav et al. 2015b) is low while the copper surface (image (b, b′) of Fig. 15) after immersion in without inhibitor 1M HCl for 24 h was damaged badly (Li et al. 2009; Wang et al. 2011). It is clearly shown in this last image that the copper sample is getting cracks as a result of the aggressiveness of the acid on the copper surface (Shukla et al. 2009), and it is covered with the striation-like corrosion products that increase surface roughness to 1.7 μm. This high roughness due to rapid corrosion in the absence of inhibitor was also observed in other works of the literature (Oguzie et al. 2007; Shukla et al. 2008). On the other hand, in the presence of inhibitor (images (c, c′) of Fig. 15) a homogeneous surface covered with grains and spherical or bread-like compounds is obtained as observed also in (Mu and Li 2005). However, the roughness of the surface layer is higher ($z = 1.9$ μm) compared to the sample copper without inhibitor. According to Parook Feroz Khan et al. (2015), the attachment of COC molecules to the copper surface appears to increase the roughness. Moreover, the resulting adsorption film (Vera et al. 2008) leads to a rough layer of precipitates responsible for slowing the corrosion process by forming a barrier to aggressive ions (Li et al. 2009) and resulting then in the high inhibition efficiency observed in this system (87%). Finally, by AFM observation, it can be concluded that the chitosan possesses a good inhibiting ability for copper corrosion in 1M HCl.

Quantum chemical calculations

Quantum chemical calculations were carried out to explain the chemical reactivity of molecular structures of corrosion inhibitors, and also to understand the process of inhibition, with thus the possible mechanism of adsorption of these molecules on the metal

surface. The Frontier molecular orbitals are very important factors in describing the interaction between the inhibitor and the metal surface. Consistent with the theory of Molecular Frontier Orbital Theory (FMO) (Khaled et al. 2009), the highest occupied molecular orbital (HOMO) is a generous system responsible for giving electrons to another recipient system, while the lowest unoccupied molecular orbital (LUMO) is an electron recipient system. The energy of gap ΔE or ($E_{HOMO} - E_{LUMO}$) makes it possible to give information on the reactivity of system; If ΔE is lower, there is the possibility of exchange of electrons between HOMO and LUMO (Alsabagh et al. 2014; Yilmaz et al. 2016). The frontiers molecule orbital density and the electrostatic potential map are plotted graphically only for gas phase; the fact is that the same forms have been found in the aqueous phases.
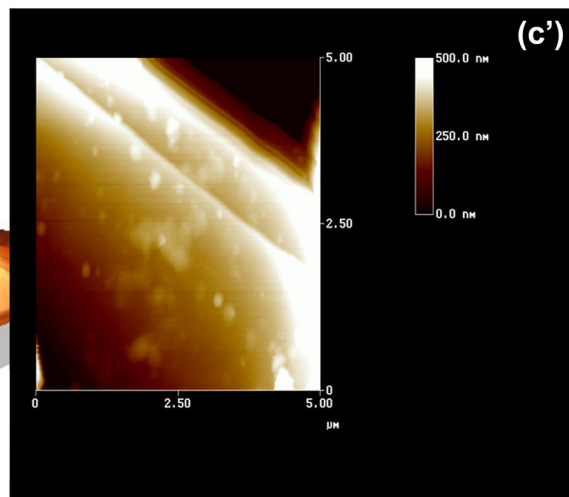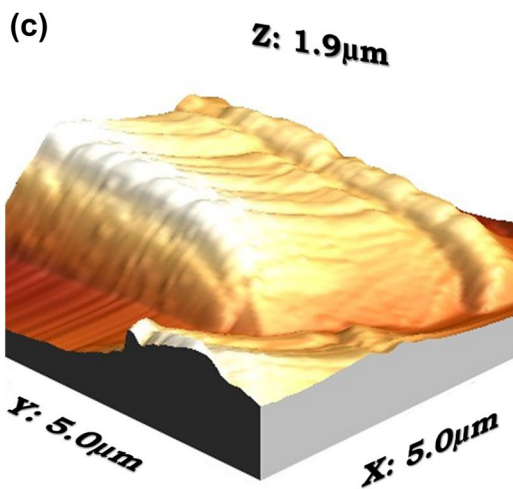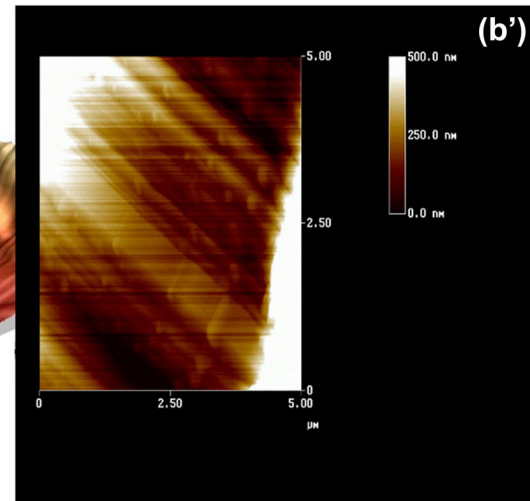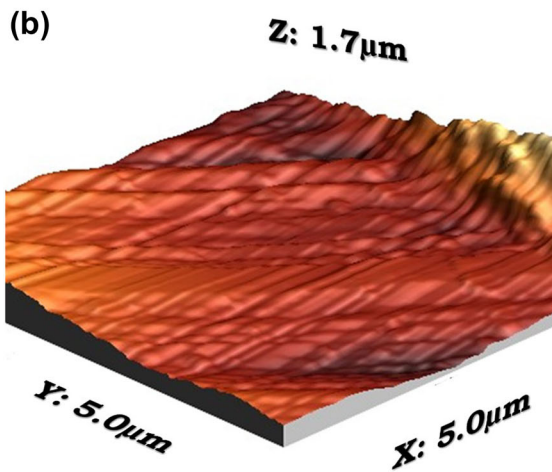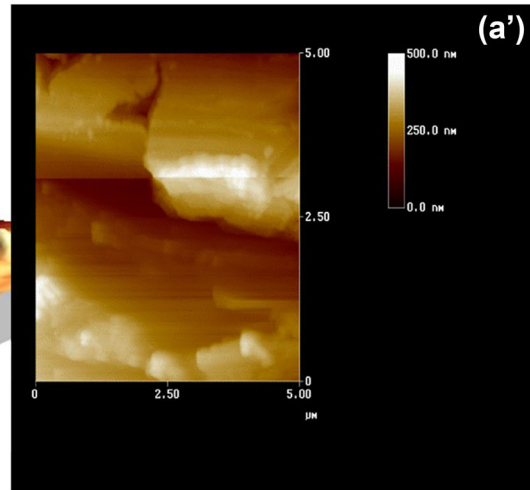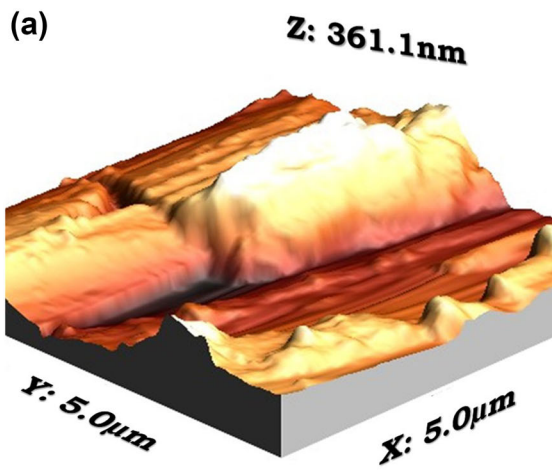
The geometry of the molecule under investigation is determined by optimizing the structural parameters B3LYP/6-31G++(2d,p) theory of the gas and aqueous phases. The geometry with the atomic numbering and the optimization energy curve for the COC molecule are presented in Fig. 16. It is shown that the stabilization of the total energy after step number 4 becomes stable at an energy value (−1183.108 Hartree). The frontier molecule orbital density distributions of HOMO and LUMO for the COC molecule are shown in Fig. 17. According to this figure, the majority of the frontier orbitals are located around the O and N atoms, which confirms the reactivity and the electronic exchange between the copper surface and the active groups of the chitosan molecule.

As seen in Tables 6 and 7 There is not much difference between the gas and aqueous phase data (Kovačević and Kokalj 2011a).The literature (Wazzan 2015; Hu et al. 2016) has confirmed that the energy of HOMO and LUMO associated with the possibility of adsorption of inhibitors at the metal interface. From Table 6 data, the important energy values of HOMO and LUMO indicate the electron exchange tendency between HOMO–LUMO of the COC and the copper (Wazzan 2015). The low energy gap ($\Delta E = 3.980(4.008)$) and the high value of dipole moment are responsible for increasing the inhibitory efficiency (El-Haddad 2013). Electronegativity χ, softness σ, and hardness η are the electronic properties of the inhibitor, according to previous studies (Yilmaz et al. 2016 and El Adnani et al. 2013), the higher value of χ and σ large and the η low mean greater inhibitory

efficiency are against copper corrosion. In our case since ΔN is positive ($\Delta N = 0.033$ (0.029)) and <3.6 According to Hu et al. (2016), if the value of ΔN is positive and <3.6, this indicates that there is an electron transfer between the metal surface and the inhibitor and, therefore, a very high inhibition efficiency.

The calculated Mulliken charges on the atoms give more information on the reactivity sites (Awad et al. 2010). The charges on the nitrogen and oxygen atoms of COC are listed in Table 7 (see Fig. 16 for atomic numbering). The highest negative charge is found on the nitrogen atoms ($N_{27} = -0.622$ (-0.690), $N_{28} = -0.588$ (-0.660)), that are responsible for the adsorption of the chitosan inhibitor to the copper surface. According to the literature, the most negatively charged atoms have the ability to exchange electrons with the positive sites of the metal (El Ibrahimi et al. 2016).

To understand the adsorption mechanism, we made a study of the electrostatic potential in the COC molecule to mention the active regions. The contour of electrostatic potential is linked to the electronic density, which is an electrostatic parameter of great importance, allowing describing the active regions of the inhibitor. Figure 18a shows the contour representation of electrostatic potential of COC. Two zones (N_{27}, O_{25}) and (N_{27}, O_{24}); the areas in red color are the negative regions and the areas in green color are the positive regions, according to this figure, it is seen that COC has several possible sites of electrophilic attack (red). The negative regions of the molecule studied were found in the tree zones (N_{27}, O_{25}), (N_{27}, O_{24}) and N_{28}; this may explain that the sites contain the N atoms, and the surroundings are richer in electron density, and are, therefore, the sites responsible for the adsorption of the chitosan molecules (Kovačević and Kokalj 2011a, b). The MEP (Molecular Electrostatic Potential mapped with Electrostatic Potential ESP) of COC was calculated at the B3LYP/6- 311G ++(2d,p) level shown in Fig. 18b. In this ca the electronic density follows in descending order in order: red > orange > yellow > green > blue. The negative regions (in yellow color) are electrophilic sites and the positive regions (in blue color) are electron-poor sites. The analysis of this figure indicates that the high electron density (yellow color) is delocalized in five electron-rich regions with nitrogen's (N_{27} and N_{28}) and oxygen's atoms (O_{24}, O_{25} and O_{36}). The rest of the

(a)

Z: 361.1nm

(a')

Y: 5.0μm

X: 5.0μm

(b)

Z: 1.7μm

(b')

Y: 5.0μm

X: 5.0μm

(c)

Z: 1.9μm

(c')

Y: 5.0μm

X: 5.0μm

◀ **Fig. 15** Two- and three-dimensional AFM images of copper specimens before and after immersion for 24 h in 1M HCl solution: (**a,a'**) reference, (**b,b'**) without inhibitor and (**c,c'**) with 10^{-1} mg/L of COC inhibitor at 25 °C

sites are characterized by low electron density. There is a concordance between the results obtained in the figures (c and d); these findings confirm the results obtained from the calculated Mulliken charges. These high density electronic atoms will create electronic interaction with the vacant d orbitals of copper, and suggests that the adsorption occurs spontaneously between COC molecules and copper (Wazzan 2015). These results confirm all that we have found in the experimental part.

Molecular dynamic simulations

As it was seen before, the copper corrosion inhibition is principally due to the adsorption of the biopolymer inhibitor on the electrode/electrolyte interface. The nature of this adsorption depends on the molecular structure of the inhibitor. To study chitosan adsorption behavior on the copper (1 1 1) surface and also for understanding the interactions between COC molecules and the metal surface, the molecular dynamics simulations are performed. Figure 19 shows the side

Fig. 17 Frontier molecule orbital density distributions of COC: **a** HOMO, **b** LUMO using the B3LYP/6-31G++(2d,p)

Fig. 16 The optimized molecular structure for chitosan compound and optimizing energy curve for this inhibitor using the B3LYP/6-31G++(2d,p)
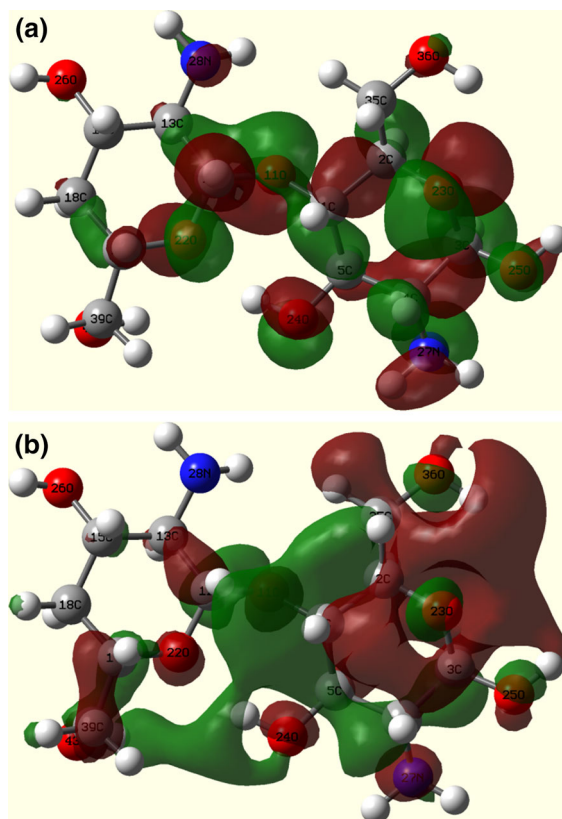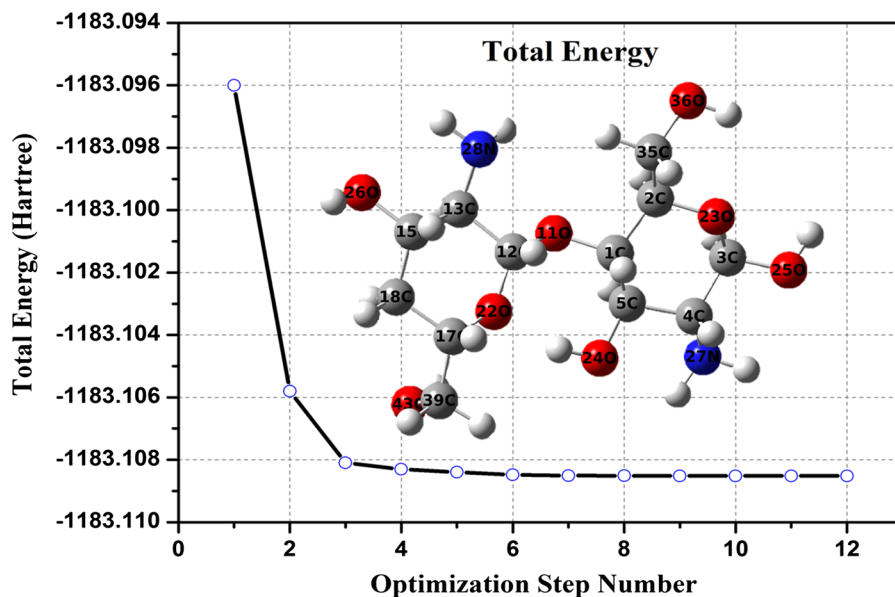
Table 6 Calculated quantum chemical parameters for the investigated inhibitor in aqueous and gas phases

Basis	Phases	ΔH (a.u)	μ (Debye)	ELUMO (eV)	EHOMO (eV)	ΔE (eV)	χ	η	σ	ΔN
6-31G++(2d,p)	Gas	−1183.108	2.754	−2.360	−6.340	3.980	4.350	1.989	0.502	0.033
	Aqueous	−1183.134	3.604	−2.359	−6.367	4.008	4.363	2.004	0.498	0.029

Table 7 Calculated charges on nitrogen and oxygen atoms of the investigated inhibitor in aqueous and gas phases

Molecule	O_{11}	O_{22}	O_{23}	O_{24}	O_{25}	O_{26}	N_{27}	N_{28}	O_{36}	O_{43}
Gas	−0.185	−0.332	−0.319	−0.527	−0.487	−0.500	−0.622	−0.588	−0.437	−0.415
Aqueous	−0.203	−0.340	−0.332	−0.569	−0.528	−0.550	−0.690	−0.660	−0.494	−0.476

Fig. 18 Electrostatic properties of chitosan (COC) at B3LYP/6-311G ++(2d,p) level, **a** the contour representation of electrostatic potential [regions of negative (positive) potential are colored *red* (*green*)], **b** molecular electrostatic potential MEP map (the electron rich region is *yellow* and the electron poor region is *blue*). (Color figure online)
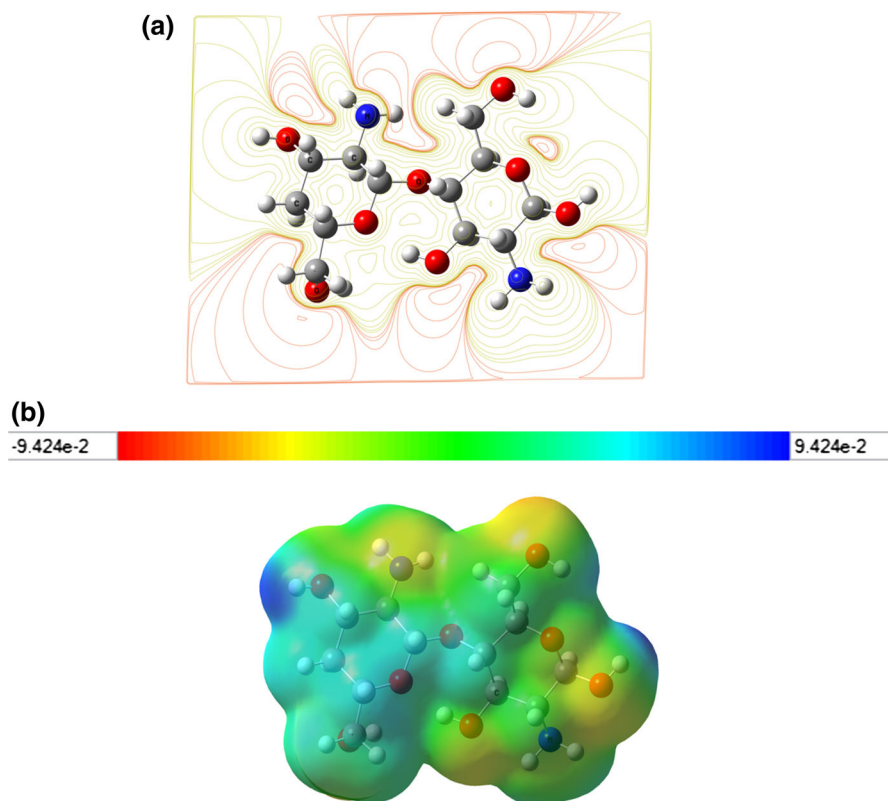
and the top views of the adsorption modeling of COC on the surface of Cu (111). According to this figure, the value of the interaction energy (i.e., binding energy) between the COC molecule and the copper surface is calculated from the following relationship:

$$E_{ads} = E_{Cu-inh} - (E_{inh} - E_{Cu}) \qquad (21)$$

where E_{inh} and E_{Cu} are the total energy of the COC and the total energy of the Cu surface, respectively.

A very wide interaction energy (i.e., binding energy) was obtained. The $E_{ads} = -E_{bind} = -263.592$ kJ/mol, which explains the spontaneity of adsorption of the chitosan molecules on the
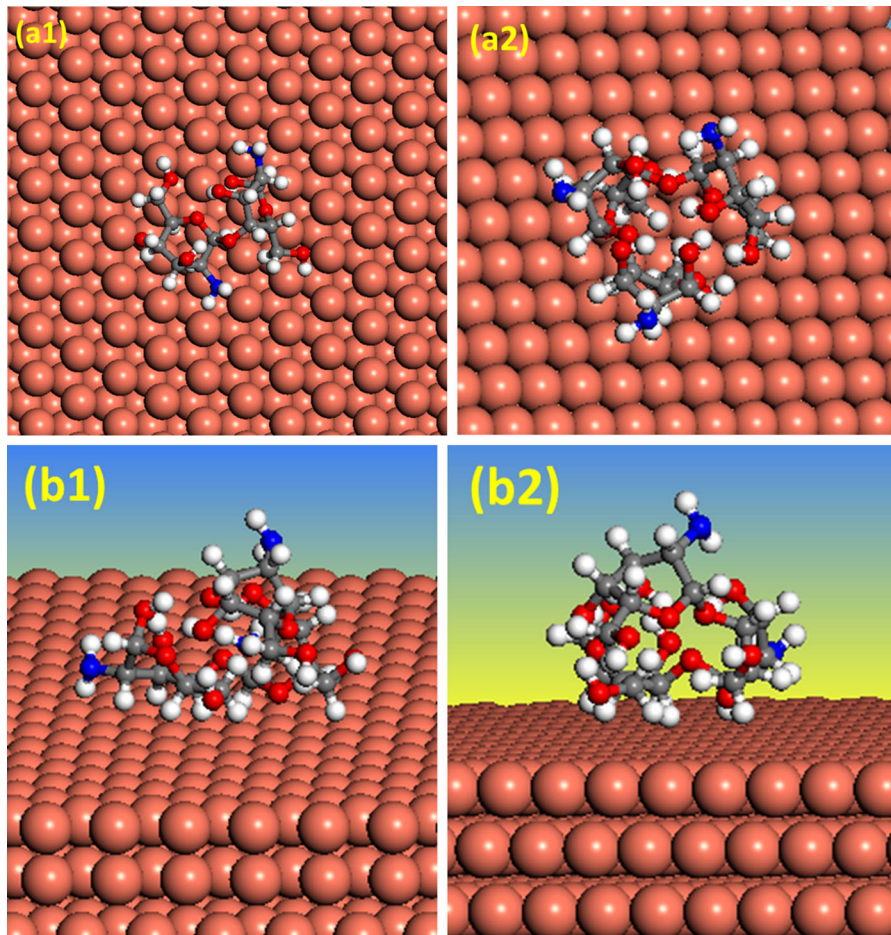
Fig. 19 Molecular simulation for the adsorption mode of chitosan inhibitor on copper (1 1 1) surface, *top view* (**a1**, **a2**) and *side view* (**b1**, **b2**)

Table 8 The adsorption and binding energies according to the number of monomer of inhibitor on copper (1 1 1) surface

Number of monomer	E_{ads}(kJ/mol)	E_{bind}(kJ/mol)
1	−163.176	163.176
2	−263.592	263.592
3	−301.248	301.248
4	−681.992	681.992
5	−790.776	790.776
6	−1004.16	1004.16
7	−1096.208	1096.208
8	−1418.376	1418.376
9	−1665.232	1665.232
10	−1560.632	1560.632

copper surface and very high inhibition efficiency (Arukalam et al. 2015).

Table 8 shows the binding and adsorption energies obtained by increasing the COC monomer, and Fig. 20 shows the variation of the binding energies with the number of monomer COC on the copper (1 1 1) surface. The adsorption energy increases with increasing monomer. This can be attributed to the increase in the functional groups of the monomer of chitosan studied, which suggests the stability and spontaneity of the complex formed (Awad et al. 2010; Awad et al. 2014; Arukalam et al. 2015).

We can draw a conclusion that the COC studied can be adsorbed on the copper surface through the

Fig. 20 The binding energies according to the number of the monomer of inhibitor on the copper (1 1 1) surface
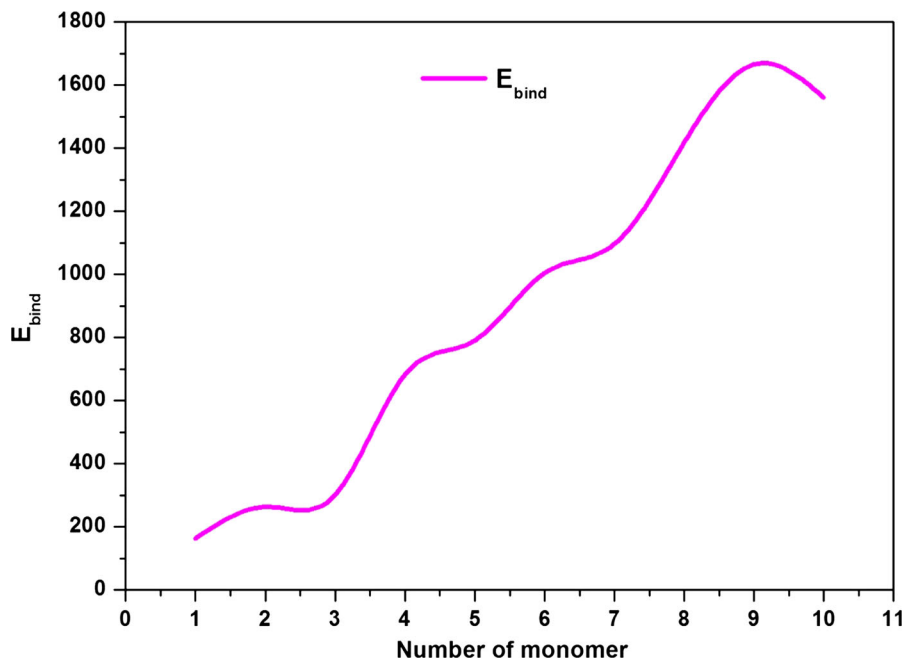
heteroatoms (N and O) of chitosan. In this way, the corrosion products formed ($CuCl$ and $CuCl_2^-$) due to the dissolution of metal in acidic medium can be prevented by the reactive effect of the COC inhibitor. These MDS results are in good agreement with our experimental results presented before.

Conclusion

Chitosan is a nontoxic biopolymer with an inhibitory effect against the copper corrosion in 1M HCl. Polarization studies revealed that COC acts as a cathodic type of inhibitor. Impedance diagrams show an increase of Rct with increasing concentration of inhibitor. The inhibitory efficiency reaches a value of 87%. The gravimetric methods are in good agreement with electrochemical methods. The adsorption of the inhibitor on the copper surface is found to obey the Langmuir adsorption isotherm type. SEM, EDX and AFM indicate that the copper dissolution is greatly mitigated by the adsorption of COC molecules on the surface forming a few layers of film. This process is responsible for blocking the formation of corrosion products. There is good agreement of the inhibition efficiencies obtained by gravimetric, dynamic polarization and EIS methods. Quantum chemical calculations have confirmed that the adsorption of the inhibitor to the surface of the metal is related with a small energy gap $\Delta E = 3.980$. The calculated Mulliken charges and the MEP mapped with Electrostatic Potential show the presence of the highest negative charges in heteroatoms nitrogen and oxygen of COC, this indicates that the chitosan inhibitor is adsorbed among these atoms on the copper surface. Molecular dynamic simulations explain the spontaneity of adsorption of the Chitosan molecules on the copper surface. These MDS calculations tests were in good agreement with experimental measurement methods.

References

Alsabagh AM, Elsabee MZ, Moustafa YM, Elfky A, Morsi RE (2014) Corrosion inhibition efficiency of some hydrophobically modified chitosan surfactants in relation to their surface active properties. Egypt J Pet 23:349–359

Antonijević MM, Milić SM, Šerbula SM, Bogdanović GD (2005) The influence of chloride ions and benzotriazole on the corrosion behavior of $Cu_{37}Zn$ brass in alkaline medium. Electrochim Acta 50:3693–3701

Antonijević MM, Milić SM, Petrović MB (2009) Films formed on copper surface in chloride media in the presence of azoles. Corros Sci 51:1228–1237

Arukalam IO, Madufor IC, Ogbobe O, Oguzie EE (2015) Inhibition of mild steel corrosion in sulfuric acid medium by hydroxyethyl cellulose. Chem Eng Commun 202:112–122

Ashassi-Sorkhabi H, Seifzadeh D, Hosseini MG (2008) EN, EIS and polarization studies to evaluate the inhibition effect of 3H-phenothiazin-3-one, 7-dimethylamin on mild steel corrosion in 1M HCl solution. Corros Sci 50:3363–3370

Awad MK, Mustafa MR, Elnga MMA (2010) Computational simulation of the molecular structure of some triazoles as inhibitors for the corrosion of metal surface. J Mol Struct (Thoechem) 959:66–74

Awad MK, Metwally MS, Soliman SA, El-Zomrawy AA, Bedair MA (2014) Experimental and quantum chemical studies of the effect of poly ethylene glycol as corrosion inhibitors of aluminum surface. J Ind Eng Chem 20:796–808

Barouni K, Bazzi L, Salghi R, Mihit M, Hammouti B, Albourine A, El Issami S (2008) Some amino acids as corrosion inhibitors for copper in nitric acid solution. Mater Lett 62:3325–3327

Bousskri A, Anejjar A, Messali M, Salghi R, Benali O, Karzazi Y, Jodeh S, Zougagh M, Ebenso EE, Hammouti B (2015) Corrosion inhibition of carbon steel in aggressive acidic media with 1-(2-(4-chlorophenyl)-2-oxoethyl)pyridazinium bromide. J Mol Liq 211:1000–1008

Cheng S, Chen S, Liu T, Chang X, Yin Y (2007) Carboxymenthylchitosan as an ecofriendly inhibitor for mild steel in 1M HCl. Mater Lett 61:3276–3280

Deyab MA, Essehli R, El Bali B (2015) Inhibition of copper corrosion in cooling seawater under flowing conditions by novel pyrophosphate. RSC Adv 5:64326–64334

El Adnani Z, McHarfi M, Sfaira M, Benzakour M, Benjelloun AT, Ebn M (2013) Touhami, DFT theoretical study of 7-R-3methylquinoxalin-2(1H)-thiones (RH; CH3; Cl) as corrosion inhibitors in hydrochloric acid. Corros Sci 68:223–230

El Ibrahimi B, Soumoue A, Jmiai A, Bourzi H, Oukhrib R, El Mouaden K, El Issami S, Bazzi L (2016) Computational study of some triazole derivatives (un- and protonated forms) and their copper complexes in corrosion inhibition process. J Mol Struct 1125:93–102

El-Haddad MN (2013) Chitosan as a green inhibitor for copper corrosion in acidic medium. Int J Biol Macromol 55:142–149

El-Haddad MN (2014) Hydroxyethylcellulose used as an eco-friendly inhibitor for 1018 c-steel corrosion in 3.5% NaCl solution. Carbohydr Polym 112:595–602

Fekry AM, Mohamed RR (2010) Acetyl thiourea chitosan as an eco-friendly inhibitor for mild steel in sulphuric acid medium. Electrochim Acta 55:1933–1939

Finšgar M, Milošev I (2010) Inhibition of copper corrosion by 1,2,3-benzotriazole: a review. Corros Sci 52:2737–2749

Frenkel D, Smit B (2002) Chapter 3—Monte Carlo simulations, understanding molecular simulation, 2nd edn. Academic Press, San Diego, pp 23–61

Frisch AMJ, Trucks GW, Schlegel HB, Scuseria GE, Robb MA, Cheeseman JR, Scalmani G, Barone V, Mennucci B,

Petersson GA, Nakatsuji H, Caricato M, Li X, Hratchian HP, Izmaylov AF, Bloino J, Zheng G, Sonnenberg JL, Hada M, Ehara M, Toyota K, Fukuda R, Hasegawa J, Ishida M, Nakajima T, Honda Y, Kitao O, Nakai H, Vreven T, Montgomery JA, JEP Jr., Ogliaro F, Bearpark M, Heyd JJ, Brothers E, Kudin KN, Staroverov VN, Kobayashi R, Normand J, Raghavachari K, Rendell A, Burant JC, Iyengar SS, Tomasi J, Cossi M, Rega N, Millam JM, Klene M, Knox JE, Cross JB, Bakken V, Adamo C, Jaramillo J, Gomperts R, Stratmann RE, Yazyev O, Austin AJ, Cammi R, Pomelli C, Ochterski JW, Martin RL, Morokuma K, Zakrzewski VG, Voth GA, Salvador P, Dannenberg JJ, Dapprich S, Daniels AD, Farkas O, Foresman JB, Ortiz JV, Cioslowski J, Fox DJ, Gaussian, Inc., Wallingford CT, 2009

Geerlings P, De Proft F, Langenaeker W (2003) Conceptual density functional theory. Chem Rev 103:1793–1874

Gomma GK (1998) Effect of azole compounds on corrosion of copper in acid medium. Mater Chem Phys 56:27–34

Habbache N, Alane N, Djerad S, Tifouti L (2009) Leaching of copper oxide with different acid solutions. Chem Eng J 152:503–508

Hassan HH, Abdelghani E, Amin MA (2007) Inhibition of mild steel corrosion in hydrochloric acid solution by triazole derivatives: part I. Polariz EIS Stud Electrochim Acta 52:6359–6366

Herreros O, Quiroz R, Viñals J (1999) Dissolution kinetics of copper, white metal and natural chalcocite in Cl_2/Cl–media. Hydrometallurgy 51:345–357

Hu K, Zhuang J, Zheng C, Ma Z, Yan L, Gu H, Zeng X, Ding J (2016) Effect of novel cytosine-L-alanine derivative based corrosion inhibitor on steel surface in acidic solution. J Mol Liq 222:109–117

Ismail KM (2007) Evaluation of cysteine as environmentally friendly corrosion inhibitor for copper in neutral and acidic chloride solutions. Electrochim Acta 52:7811–7819

Khaled KF (2010) Corrosion control of copper in nitric acid solutions using some amino acids—a combined experimental and theoretical study. Corros Sci 52:3225–3234

Khaled KF, Hackerman N (2004) Ortho-substituted anilines to inhibit copper corrosion in aerated 0.5M hydrochloric acid. Electrochim Acta 49:485–495

Khaled KF, Fadl-Allah SA, Hammouti B (2009) Some benzotriazole derivatives as corrosion inhibitors for copper in acidic medium: experimental and quantum chemical molecular dynamics approach. Mater Chem Phys 117:148–155

Khan PF, Shanthi V, Babu RK, Muralidharan S, Barik RC (2015) Effect of benzotriazole on corrosion inhibition of copper under flow conditions. J Environ Chem Eng 3:10–19

Kim E-Y, Kim M-S, Lee J-C, Jeong J, Pandey BD (2011) Leaching kinetics of copper from waste printed circuit boards by electro-generated chlorine in HCl solution. Hydrometallurgy 107:124–132

Kirkpatrick S, Gelatt CD, Vecchi MP (1983) Optimization by simulated annealing. Science 220:671–680

Kovačević N, Kokalj A (2011a) Analysis of molecular electronic structure of imidazole- and benzimidazole-based inhibitors: a simple recipe for qualitative estimation of chemical hardness. Corros Sci 53:909–921

Kovačević N, Kokalj A (2011b) DFT study of interaction of azoles with Cu(111) and Al(111) surfaces: role of azole nitrogen atoms and dipole–dipole interactions. J Phys Chem C 115:24189–24197

Larabi L, Benali O, Mekelleche SM, Harek Y (2006) 2-Mercapto-1-methylimidazole as corrosion inhibitor for copper in hydrochloric acid. Appl Surf Sci 253:1371–1378

Lebrini M, Lagrenée M, Vezin H, Gengembre L, Bentiss F (2005) Electrochemical and quantum chemical studies of new thiadiazole derivatives adsorption on mild steel in normal hydrochloric acid medium. Corros Sci 47:485–505

Lee C, Yang W, Parr RG (1988) Development of the Colle-Salvetti correlation-energy formula into a functional of the electron density. Phys Rev B 37:785–789

Li X, Deng S, Fu H (2009) Synergistic inhibition effect of red tetrazolium and uracil on the corrosion of cold rolled steel in H_3PO_4 solution: weight loss, electrochemical, and AFM approaches. Mater Chem Phys 115:815–824

Liao QQ, Yue ZW, Yang D, Wang ZH, Li ZH, Ge HH, Li YJ (2011) Self-assembled monolayer of ammonium pyrrolidine dithiocarbamate on copper detected using electrochemical methods, surface enhanced Raman scattering and quantum chemistry calculations. Thin Solid Films 519:6492–6498

Liu Y, Zou C, Yan X, Xiao R, Wang T, Li M (2015) β-Cyclodextrin modified natural chitosan as a green inhibitor for carbon steel in acid solutions. Ind Eng Chem Res 54:5664–5672

Menaka R, Subhashini S (2016) Chitosan Schiff base as eco-friendly inhibitor for mild steel corrosion in 1M HCl. J Adhes Sci Technol 30:1622–1640

Mourya P, Banerjee S, Singh MM (2014) Corrosion inhibition of mild steel in acidic solution by *Tagetes erecta* (Marigold flower) extract as a green inhibitor. Corros Sci 85:352–363

Mu G, Li X (2005) Inhibition of cold rolled steel corrosion by Tween-20 in sulfuric acid: weight loss, electrochemical and AFM approaches. J Colloid Interface Sci 289:184–192

Núñez L, Reguera E, Corvo F, González E, Vazquez C (2005) Corrosion of copper in seawater and its aerosols in a tropical island. Corros Sci 47:461–484

Oguzie EE, Li Y, Wang FH (2007) Corrosion inhibition and adsorption behavior of methionine on mild steel in sulfuric acid and synergistic effect of iodide ion. J Colloid Interface Sci 310:90–98

Pearson RG (1988) Absolute electronegativity and hardness: application to inorganic chemistry. Inorg Chem 27:734–740

Rhazi M, Desbrières J, Tolaimate A, Rinaudo M, Vottero P, Alagui A, El Meray M (2002) Influence of the nature of the metal ions on the complexation with chitosan.: application to the treatment of liquid waste. Eur Polym J 38:1523–1530

Rocca E, Bertrand G, Rapin C, Labrune JC (2001) Inhibition of copper aqueous corrosion by non-toxic linear sodium heptanoate: mechanism and ECAFM study. J Electroanal Chem 503:133–140

Sangeetha Y, Meenakshi S, SairamSundaram C (2015) Corrosion mitigation of N-(2-hydroxy-3-trimethyl ammonium)propyl chitosan chloride as inhibitor on mild steel. Int J Biol Macromol 72:1244–1249

Sangeetha Y, Meenakshi S, Sairam Sundaram C (2016) Investigation of corrosion inhibitory effect of hydroxyl propyl alginate on mild steel in acidic media. J Appl Polym Sci 133 n/a-n/a

Sangeetha Y, Meenakshi S, Sairam Sundaram C (2016b) Corrosion inhibition of aminated hydroxyl ethyl cellulose on mild steel in acidic condition. Carbohydr Polym 150:13–20

Satapathy AK, Gunasekaran G, Sahoo SC, Amit K, Rodrigues PV (2009) Corrosion inhibition by Justicia gendarussa plant extract in hydrochloric acid solution. Corros Sci 51:2848–2856

Sherif EM, Park S-M (2006a) Inhibition of copper corrosion in acidic pickling solutions by N-phenyl-1,4-phenylenediamine. Electrochim Acta 51:4665–4673

Sherif EM, Park S-M (2006b) Effects of 2-amino-5-ethylthio-1,3,4-thiadiazole on copper corrosion as a corrosion inhibitor in aerated acidic pickling solutions. Electrochim Acta 51:6556–6562

Sherif EM, Park S-M (2006c) 2-Amino-5-ethyl-1,3,4-thiadiazole as a corrosion inhibitor for copper in 3.0% NaCl solutions. Corros Sci 48:4065–4079

Sherif E-SM, Erasmus RM, Comins JD (2007) Effects of 3-amino-1,2,4-triazole on the inhibition of copper corrosion in acidic chloride solutions. J Colloid Interface Sci 311:144–151

Sherif E-SM, Erasmus RM, Comins JD (2008) Inhibition of copper corrosion in acidic chloride pickling solutions by 5-(3-aminophenyl)-tetrazole as a corrosion inhibitor. Corros Sci 50:3439–3445

Shukla SK, Quraishi MA, Prakash R (2008) A self-doped conducting polymer "polyanthranilic acid": an efficient corrosion inhibitor for mild steel in acidic solution. Corros Sci 50:2867–2872

Shukla SK, Singh AK, Ahamad I, Quraishi MA (2009) Streptomycin: a commercially available drug as corrosion inhibitor for mild steel in hydrochloric acid solution. Mater Lett 63:819–822

Simonović AT, Petrović MB, Radovanović MB, Milić SM, Antonijević MM (2014) Inhibition of copper corrosion in acidic sulphate media by eco-friendly amino acid compound. Chem Pap 68:362–371

Subramanian R, Lakshminarayanan V (2002) Effect of adsorption of some azoles on copper passivation in alkaline medium. Corros Sci 44:535–554

Suzuki S, Shibutani N, Mimura K, Isshiki M, Waseda Y (2006) Improvement in strength and electrical conductivity of Cu–Ni–Si alloys by aging and cold rolling. J Alloys Compd 417:116–120

Tan YS, Srinivasan MP, Pehkonen SO, Chooi SYM (2006) Effects of ring substituents on the protective properties of self-assembled benzenethiols on copper. Corros Sci 48:840–862

Tawfik SM (2015) Alginate surfactant derivatives as an eco-friendly corrosion inhibitor for carbon steel in acidic environments. RSC Adv 5:104535–104550

Tromans D, SiIva JC (1996) Anodic behavior of copper in iodide solutions. J Electrochem Soc 143:458–465

Umoren SA, Eduok UM (2016) Application of carbohydrate polymers as corrosion inhibitors for metal substrates in different media: a review. Carbohydr Polym 140:314–341

Vathsala K, Venkatesha TV, Praveen BM, Nayana KO (2010) Electrochemical generation of Zn-chitosan composite

coating on mild steel and its corrosion studies. Engineering 2:580–584

Vera R, Bastidas F, Villarroel M, Oliva A, Molinari A, Ramírez D, del Río R (2008) Corrosion inhibition of copper in chloride media by 1,5-bis(4-dithiocarboxylate-1-dodecyl-5-hydroxy-3-methylpyrazolyl)pentane. Corros Sci 50:729–736

Wang B, Du M, Zhang J, Gao CJ (2011) Electrochemical and surface analysis studies on corrosion inhibition of Q235 steel by imidazoline derivative against CO_2 corrosion. Corros Sci 53:353–361

Wang H-X, Zhang Y, Cheng J-L, Li Y-S (2015) High temperature oxidation resistance and microstructure change of aluminized coating on copper substrate. Trans Nonferrous Met Soc China 25:184–190

Wazzan NA (2015) DFT calculations of thiosemicarbazide, arylisothiocynates, and 1-aryl-2,5-dithiohydrazodicarbonamides as corrosion inhibitors of copper in an aqueous chloride solution. J Ind Eng Chem 26:291–308

Yadav M, Kumar S, Sinha RR, Bahadur I, Ebenso EE (2015a) New pyrimidine derivatives as efficient organic inhibitors on mild steel corrosion in acidic medium: electrochemical, SEM, EDX, AFM and DFT studies. J Mol Liq 211:135–145

Yadav M, Sinha RR, Sarkar TK, Bahadur I, Ebenso EE (2015b) Application of new isonicotinamides as a corrosion inhibitor on mild steel in acidic medium: electrochemical, SEM, EDX, AFM and DFT investigations. J Mol Liq 212:686–698

Yilmaz N, Fitoz A, Ergun Ü, Emregül KC (2016) A combined electrochemical and theoretical study into the effect of 2-((thiazole-2-ylimino)methyl)phenol as a corrosion inhibitor for mild steel in a highly acidic environment. Corros Sci 111:110–120

Zhang D-Q, Gao L-X, Zhou G-D (2005) Inhibition of copper corrosion in aerated hydrochloric acid solution by amino-acid compounds. J Appl Electrochem 35:1081–1085

Zhang D-Q, Cai Q-R, He X-M, Gao L-X, Zhou G-D (2008a) Inhibition effect of some amino acids on copper corrosion in HCl solution. Mater Chem Phys 112:353–358

Zhang D-Q, Cai Q-R, Gao L-X, Lee KY (2008b) Effect of serine, threonine and glutamic acid on the corrosion of copper in aerated hydrochloric acid solution. Corros Sci 50:3615–3621

Zhang P, Zhu Q, Su Q, Guo B, Cheng S-K (2016) Corrosion behavior of T2 copper in 3.5% sodium chloride solution treated by rotating electromagnetic field. Trans Nonferrous Met Soc China 26:1439–1446